Crimson Publishers
Wings to the Research

Research Article

Multi-Sensor Remote Sensing for Hydrothermal Alteration Mapping and Copper Prospectivity in the Skardu Region, Pakistan

ISSN: 2578-0255

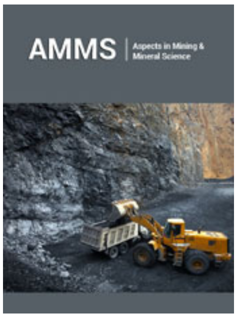

Zakaria Hussain[1], Jaffer Raza[2], Zeenat Khan[3]*, Gulzaib Jahangir[4], Basir Ali[5] and Mahin Jamil[6]

[1]Department of Earth Sciences, Quaid-e-Azam University, Pakistan

[2]University of Azad Jammu and Kashmir, Pakistan

[3]Research Analyst, Al-Mussawir Engineers, Pakistan

[4]Pir Mehr Ali Shah Arid Agriculture University, Pakistan

[5]Department of Geography and Geomatics, University of Peshawar, Pakistan

[6]Department of Civil Engineering, University of Engineering and Technology (UET), Pakistan

***Corresponding author:** Zeenat Khan, Research Analyst, Al-Mussawir Engineers, Rawalpindi, Pakistan

Submission: June 22, 2026
Published: July 27, 2026

Volume 15 - Issue 2

How to cite this article: Zakaria Hussain, Jaffer Raza, Zeenat Khan*, Gulzaib Jahangir, Basir Ali and Mahin Jamil. Multi-Sensor Remote Sensing for Hydrothermal Alteration Mapping and Copper Prospectivity in the Skardu Region, Pakistan. Aspects Min Miner Sci. 15(2). AMMS. 000860. 2026.
DOI: 10.31031/AMMS.2026.15.000860

Abstract

Hydrothermal alteration minerals are important indicators of copper mineralization, but their reliable detection in rugged mountainous terrains remains challenging because of spectral mixing, complex geological settings, and limited field accessibility. This study presents an integrated multi-sensor remote sensing framework for hydrothermal alteration mapping and copper prospectivity assessment in District Skardu, Gilgit-Baltistan, Pakistan, within the Karakoram orogenic belt. ASTER, Sentinel-2A, and Landsat-8 datasets were integrated using diagnostic band-ratio indices and Spectral Angle Mapper (SAM) classification to delineate quartz, clay, carbonate, and iron-oxide alteration assemblages. Mineral endmembers derived from the USGS Spectral Library were used to classify alunite, kaolinite, illite, hematite, goethite, dolomite, calcite, epidote, and quartz. The results demonstrate the superior performance of ASTER for hydrothermal alteration mapping, identifying substantially larger and more spatially coherent alteration zones, including alunite (43.04km^2), calcite (28.81km^2), dolomite (159.28km^2), epidote (176.86km^2), goethite (432.02km^2), hematite (244.11km^2), kaolinite (51.84km^2), and quartz (77.17km^2), compared with Landsat-8. Band-ratio analysis further showed that ASTER mapped a larger quartz-rich area (127.95km^2), whereas Sentinel-2A more effectively delineated clay-rich zones (82.08km^2), highlighting the complementary strengths of high spectral and high spatial resolution sensors. Validation using field observations and the Shahzad International Pvt. Ltd. mining lease at Shigri Balla demonstrated strong spatial correspondence between mapped alteration zones and known mineralized areas. Unlike previous studies that primarily relied on individual ASTER or Sentinel imagery for hydrothermal alteration mapping, this study integrates ASTER, Sentinel-2A, and Landsat-8 within a unified framework combining spectral indices, SAM classification, and field validation to improve the reliability of hydrothermal alteration mapping and copper prospectivity assessment in the complex Himalayan terrain of northern Pakistan. This integrated workflow provides a cost-effective, scalable, and reproducible approach for regional mineral exploration in remote and tectonically active regions.

Keywords: Hydrothermal alteration; Copper prospectivity; ASTER SWIR; Spectral angle mapper (SAM); Sentinel-2A; Multi sensor remote sensing

Introduction

Remote sensing has become an essential technology in modern mineral exploration, especially in tectonically active and inaccessible mountainous regions. Multispectral satellite systems enable detection of diagnostic spectral responses of surface minerals associated with hydrothermal ore-forming environments [1]. Alteration minerals such as kaolinite, illite, alunite, hematite, and goethite act as reliable surface indicators of subsurface mineralization processes and exhibit diagnostic absorption features in visible, near-infrared, and shortwave infrared spectral regions [2]. District Skardu in Gilgit-Baltistan lies within a structurally complex segment of the Karakoram orogenic belt characterized by active tectonics and diverse lithology [3]. Field-based geological exploration in this region is highly constrained due to rugged topography, extreme altitude, and harsh climatic conditions [4]. As a result, remote sensing provides a cost-effective and scalable alternative for preliminary mineral exploration and regional mapping [5]. However, single-sensor approaches often fail to fully capture the complexity of hydrothermal alteration systems in mountainous terrains due to spectral mixing and resolution limitations [6]. This study integrates ASTER, Sentinel-2A, and Landsat-8 datasets to improve spectral discrimination and enhance alteration mapping accuracy in Skardu [7]. The main objective is to develop a robust multi-sensor framework for identifying copper-associated hydrothermal zones in complex geological settings [8].

This integrated approach strengthens geological interpretation by combining complementary spectral and spatial sensor capabilities. Hydrothermal alteration systems are key indicators of porphyry copper mineralization due to fluid-rock interactions during ore formation [9]. These systems typically produce zoned alteration assemblages including argillic, phyllic, and propylitic types, each characterized by distinct spectral signatures in the shortwave infrared region [10]. Such minerals exhibit diagnostic absorption features that can be effectively detected using multispectral remote sensing techniques [11]. ASTER is particularly effective for mineral discrimination due to its six SWIR bands covering key absorption wavelengths associated with alteration minerals [12]. Landsat-8 provides broader spectral and thermal coverage useful for regional geological interpretation and structural analysis [13]. Sentinel-2A offers high spatial resolution imagery but has limited SWIR capability for detailed mineral separation [14]. Each dataset therefore provides partial but incomplete information when used independently in structurally complex terrains [15]. Previous studies have shown partial success in single-sensor mineral mapping but highlight limitations in spectral discrimination and mapping accuracy [16]. Multi-sensor integration remains underexplored for copper exploration in Himalayan tectonic environments [17]. This study addresses this gap by integrating complementary satellite datasets into a unified analytical framework [18]. The approach enhances reliability and reduces uncertainty in hydrothermal alteration detection across complex terrains.

Recent advances in remote sensing have significantly improved hydrothermal alteration mapping and mineral prospectivity assessment through the integration of multispectral satellite data and advanced image processing techniques [19]. Studies conducted between 2022 and 2026 consistently demonstrate that ASTER remains the most effective multispectral sensor for discriminating hydroxyl-bearing, carbonate, and silica-rich alteration minerals because of its six SWIR bands, whereas Sentinel-2 provides superior spatial resolution for delineating surface alteration patterns, and Landsat-8/9 contributes valuable regional geological information and long-term temporal coverage [20].

Recent investigations have employed image fusion, Principal Component Analysis (PCA), band ratios, Spectral Angle Mapper (SAM), matched filtering, and deep learning algorithms to enhance hydrothermal alteration mapping and mineral exploration [21]. Nevertheless, most studies have focused on either single-sensor datasets or limited sensor combinations and have frequently relied on additional airborne geophysical datasets or artificial intelligence models that may not be readily applicable in data-scarce mountainous regions. Consequently, challenges associated with spectral mixing, transferability, and robust field validation remain unresolved, particularly in structurally complex terrains such as the Himalayan and Karakoram orogenic belts [22,23]. A critical comparison of representative studies published between 2022 and 2026 (Table 1) highlights these methodological advances while revealing the limited application of an integrated ASTER-Sentinel-2A-Landsat-8 workflow that combines diagnostic band-ratio analysis, Spectral Angle Mapper (SAM) classification, and field validation for copper prospectivity mapping [24]. Therefore, this study addresses an important research gap by developing a unified, multi-sensor framework that exploits the complementary spectral and spatial capabilities of the three satellite systems to improve hydrothermal alteration mapping in the tectonically complex terrain of northern Pakistan.

Table 1: Comparison of recent studies (2022-2026) on hydrothermal alteration mapping.

Year	Study Area	Sensors	Methodology	Key Findings	Limitation	Reference
2022	Pulang Cu Deposit, China	ASTER+Sentinel-2	Image fusion (HPF, PCA), spectral matching	Fusion improved hydrothermal alteration mapping over ASTER alone.	No Landsat integration or unified workflow.	[19]
2022	Takab-Baneh, Iran	ASTER	MNF, PPI, MTMF, PCA, Band Ratios	ASTER SWIR successfully discriminated alteration minerals.	Single-sensor approach only.	[20]
2023	Eastern Desert, Egypt	ASTER+Sentinel-2+Landsat-8 EO-1 ALI	Band ratios, PCA, geophysical integration	Multi-source integration improved alteration mapping accuracy.	Required airborne geophysical datasets.	[21]
2024	Brazil	ASTER+Sentinel-2	PCA, entropy analysis	Demonstrated complementary performance of ASTER and Sentinel-2 for hydrothermal alteration mapping.	No SAM classification or field validation.	[22]

2024	Igarra Schist Belt, Nigeria	ASTER+Airborne Radiometric Data	Band ratios, FCC, radiometric interpretation	Integration enhanced alteration zone identification.	Depended on airborne datasets rather than satellite-only workflow.	[23]
2025	Fatira Mine, Egypt	Landsat-8+ASTER+Sentinel-2	Machine learning+field mineralogy	Improved mapping of alteration zones using multisensor imagery and AI.	Focused on gold mineralization rather than copper prospectivity.	[24]
2025	Anti-Atlas, Morocco	ASTER	SFF, MF, LS-Fit, CEM	Successfully mapped argillic, phyllic, propylitic and iron-oxide alteration.	Used only ASTER; no multisensor integration.	[25]
2025	Coastal Cordillera, Chile	ASTER+Sentinel-2+Landsat-9	Band ratios, DPCA, SAM	Three-sensor integration improved mapping of porphyry copper-related alteration minerals.	Conducted in Chile; applicability to Himalayan terrain not assessed.	[26]
2026	Zafarghand, Iran	Sentinel-2	β-VAE, DWT, Gaussian Mixture Model	Deep learning enhanced Sentinel-2-based hydrothermal alteration and iron mineral mapping.	No ASTER or Landsat comparison; focused on AI classification.	[27]

Despite significant advances in hydrothermal alteration mapping, several important challenges remain unresolved. Most recent studies have focused on individual satellite sensors or limited multisensor combinations and have been conducted in relatively well-characterized mining districts outside the Himalayan region. Consequently, the transferability of these approaches to the tectonically complex Karakoram orogenic belt remains uncertain due to rugged topography, heterogeneous lithology, spectral mixing, and limited field accessibility [7].

Furthermore, few studies have integrated the complementary spectral capabilities of ASTER, the high spatial resolution of Sentinel-2A, and the regional geological coverage of Landsat-8 within a single, field-validated framework for copper prospectivity assessment [24-27]. Therefore, there remains a need for a robust, cost-effective, and reproducible multisensor methodology capable of improving hydrothermal alteration mapping in remote mountainous environments. This study addresses this gap by developing and validating an integrated remote sensing framework for identifying copper-associated hydrothermal alteration zones in District Skardu, northern Pakistan.

Geologically, District Skardu is located within the collision zone between the Indian and Eurasian plates characterized by intense deformation, thrusting, folding, and intrusive activity [28]. This tectonic setting has generated extensive fault systems and hydrothermal pathways that facilitate fluid circulation and mineral deposition [29]. The region consists of metamorphic rocks such as schists and gneisses along with igneous and sedimentary formations [30]. These lithological units provide a favorable structural environment for copper mineralization and hydrothermal alteration processes [31]. Copper-bearing minerals such as chalcopyrite, malachite, and azurite are commonly associated with these alteration zones [32]. However, strong topographic relief and structural complexity create significant spectral mixing challenges in remote sensing interpretation [33]. Traditional field mapping is limited due to inaccessibility, high elevation, and logistical constraints [34].

Therefore, satellite-based mineral mapping becomes essential for regional exploration in such environments [35]. Techniques such as band ratioing and Spectral Angle Mapper classification improve detection of alteration minerals [36]. These methods enable systematic identification of hydrothermal alteration zones linked to ore-forming processes [37]. The geological complexity of Skardu makes it an ideal natural laboratory for integrated remote sensing analysis. Motivated by the identified research gap, the primary objective of this study is to develop and validate an integrated multi-sensor remote sensing framework for hydrothermal alteration mapping and copper prospectivity assessment in District Skardu using ASTER, Sentinel-2A, and Landsat-8 datasets. The methodology combines spectral preprocessing, band ratio analysis, and Spectral Angle Mapper classification to enhance mineral detection accuracy across multiple spatial and spectral scales. Diagnostic spectral indices are applied to highlight quartz, carbonate, and clay alteration zones associated with hydrothermal systems. SAM classification is performed using USGS spectral libraries to ensure standardized and reliable mineral identification. Ground truth validation is incorporated using known mining lease boundaries and field observations from hydrothermally altered zones. Comparative analysis evaluates the performance of each sensor in terms of spectral discrimination and spatial mapping capability. ASTER provides high spectral resolution suitable for detailed mineral identification, Sentinel-2A offers fine spatial resolution for structural interpretation, and Landsat-8 ensures regional-scale geological coverage. The integration of these datasets enables multi-scale interpretation of hydrothermal systems and reduces uncertainty associated with single-sensor analysis. The novelty of this study lies in the systematic fusion of three complementary satellite datasets for copper alteration mapping in a complex Himalayan terrain. The findings demonstrate improved accuracy in delineating hydrothermal alteration zones compared to individual sensor approaches. Overall, this research establishes a scalable, reliable, and cost-effective framework for copper exploration in structurally complex mountainous environments.

Materials and Methods

Study area

District Skardu, located in Gilgit-Baltistan, northern Pakistan, constitutes a tectonically active segment of the Karakoram orogenic belt and represents a high-potential metallogenic province for copper-associated mineralization. The region is characterized by extreme topographic variability, with elevations ranging from ~2,200m to >5,000m above sea level, forming deeply incised valleys and structurally controlled high-relief mountain systems (Figure 1). Climatically, Skardu is dominated by a cold-arid regime with minimal precipitation and sparse vegetation cover, conditions that significantly enhance lithological exposure and improve the effectiveness of optical remote sensing for bedrock characterization. Structurally, the study area lies within the India-Eurasia collision zone, where ongoing crustal convergence has generated a complex deformational architecture comprising thrust systems, fold belts, and brittle-ductile shear zones. This tectonic framework has played a critical role in channeling hydrothermal fluids and facilitating ore-forming processes. Lithologically, the region comprises high-grade metamorphic units (schists and gneisses), intrusive igneous bodies (granites and diorites), and subordinate sedimentary sequences, collectively forming a favorable geological environment for hydrothermal mineralization systems.

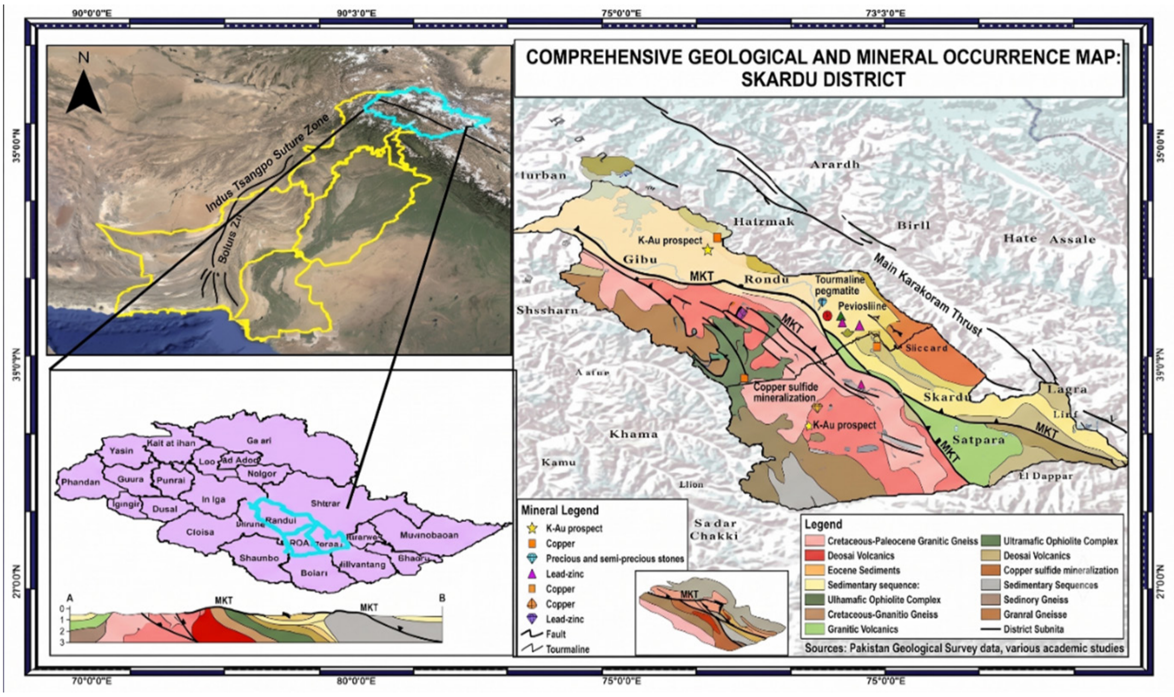

Figure 1: Geographic location and geological setting of the study area, District Skardu, Gilgit-Baltistan, Pakistan.

Previous geological investigations have documented widespread occurrences of copper-associated mineral phases, including chalcopyrite, malachite, and azurite, typically occurring within structurally controlled alteration zones. However, the extreme terrain complexity, limited accessibility, and logistical constraints severely restrict systematic field-based mapping and sampling campaigns. Consequently, Skardu represents an ideal natural laboratory for evaluating advanced remote sensing-based mineral exploration methodologies. Overall, the study area provides a structurally and lithologically optimal setting for multi-sensor hydrothermal alteration mapping.

Data acquisition

A multi-source remote sensing dataset was assembled to enable robust characterization of hydrothermal alteration signatures and associated lithological variability in District Skardu. Freely available multispectral satellite datasets, including ASTER Level-1T, Sentinel-2A Multispectral Instrument (MSI), and Landsat-8 Operational Land Imager (OLI)/Thermal Infrared Sensor (TIRS), were selected because of their complementary spectral and spatial characteristics for hydrothermal alteration mapping. The spectral bands, spatial resolution, primary applications, and data sources of the selected datasets are summarized in Table 2. Image selection prioritized cloud-free or minimally cloud-contaminated scenes acquired under favorable atmospheric conditions to maximize lithological exposure and minimize spectral interference. The selected datasets represent comparable seasonal conditions to ensure spectral consistency during multisensor integration. ASTER Level-1T imagery was acquired with primary emphasis on the Shortwave Infrared (SWIR) bands (Bands 4-9), which are highly sensitive to the diagnostic absorption features of hydroxyl-bearing, carbonate, and silica-rich alteration minerals. Sentinel-2A multispectral imagery was incorporated because of its high spatial resolution (10-20m) and the availability of visible, red-edge, Near-Infrared (NIR), and SWIR bands, enabling vegetation suppression, iron-oxide enhancement, and lithological discrimination. Landsat-8 OLI/TIRS data were integrated to provide complementary spectral and thermal information, supporting regional-scale lithological mapping, structural interpretation, and thermal anomaly analysis. To strengthen geological interpretation, ancillary datasets, including regional lithological maps obtained from the Geological Survey of Pakistan and documented mineral occurrence records (chalcopyrite, malachite, and azurite), were incorporated. GPS-referenced field observations collected during reconnaissance surveys were further used for spatial validation and georeferencing refinement. The integration of multisource satellite imagery with geological and field datasets provided a comprehensive and cost-effective framework for hydrothermal alteration mapping in the structurally complex terrain of the Karakoram orogenic belt.

Table 2: Characteristics of the multispectral satellite datasets used for hydrothermal alteration mapping in this study.

Dataset	Product	Spectral Bands Used	Spatial Resolution	Primary Purpose	Data Source
ASTER	Level-1T	VNIR (1-3), SWIR (4-9)	15m (VNIR), 30m (SWIR)	Hydroxyl-, carbonate-, and silica-rich mineral discrimination	NASA LP DAAC
Sentinel-2A MSI	Level-1C/Level-2A*	Bands 2-8A, 11, 12	10-20m	High-resolution lithological and alteration mapping	Copernicus Data Space
Landsat-8 OLI/TIRS	OLI/TIRS	Bands 2-7, 10-11	30m (OLI), 100m (TIRS)	Regional lithological and thermal analysis	USGS Earth Explorer

Preprocessing

All datasets were subjected to a standardized preprocessing workflow implemented in ENVI to ensure radiometric consistency, atmospheric correction, and geometric harmonization across sensors. Raw digital numbers were first converted to at-sensor radiance and subsequently transformed into surface reflectance to facilitate reliable inter-sensor spectral comparison. Atmospheric correction of ASTER and Landsat-8 imagery was performed using the Fast Line-of-sight Atmospheric Analysis of Spectral Hypercubes (FLAASH) module in ENVI, whereas Sentinel-2A imagery was processed using the Sen2Cor processor to generate Level-2A surface reflectance products. Following atmospheric correction, all datasets were geometrically co-registered to the WGS 84/UTM Zone 43N coordinate reference system to ensure pixel-level alignment across sensors prior to multisensor integration. Following correction, spectral bands were systematically stacked to generate multispectral composites optimized for mineral detection. ASTER VNIR and SWIR bands were integrated, while Sentinel-2A bands 2-8A, 11, and 12 were included to capture diagnostic reflectance variations across visible and SWIR domains. Landsat-8 bands 2-7 and thermal bands 10-11 were incorporated to support lithological discrimination and thermal response analysis. The overall methodological workflow adopted in this study, from data acquisition and preprocessing to spectral analysis, mineral classification, and validation, is illustrated in Figure 2.

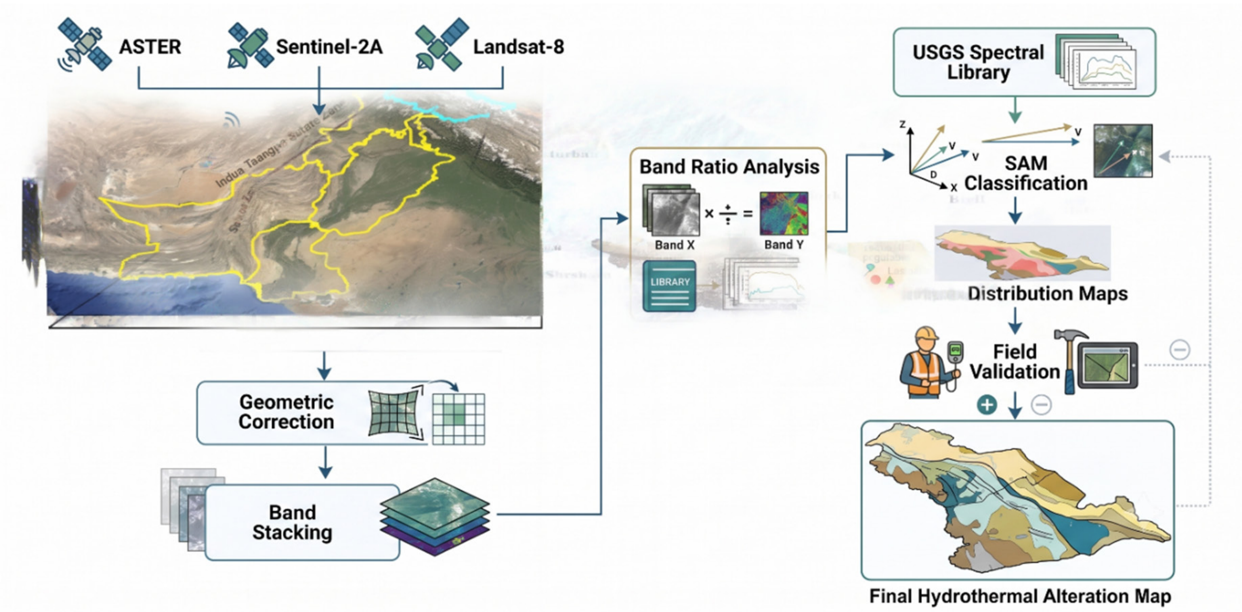

Figure 2: Workflow of the proposed multi-sensor remote sensing methodology for hydrothermal alteration mapping and copper prospectivity assessment.

Spectral analysis

Spectral analysis was conducted using a hybrid approach combining targeted band-ratio enhancement techniques and Spectral Angle Mapper (SAM) classification to delineate hydrothermal alteration mineral assemblages. Band-ratio composites were designed to amplify diagnostic spectral contrasts associated with iron oxides, phyllosilicates, carbonates, and silica-rich lithologies. Iron oxide mineralization was enhanced using ASTER band ratio 2/1 and Landsat-8 band ratio 4/2, which are widely used to emphasize ferric iron-bearing minerals due to their diagnostic spectral characteristics in the visible region [38]. Clay and hydroxyl-bearing minerals were highlighted using ASTER band ratio 4/7 and Landsat-8 band ratio 6/7, exploiting the characteristic Al-OH absorption features within the shortwave infrared region [39]. Quartz-rich and silicified zones were delineated using the ASTER 7/6 ratio, which enhances silica-rich lithologies and hydrothermal alteration associated with porphyry mineral systems [40]. SAM classification was implemented using mineral endmember spectra obtained from the USGS Spectral Library to ensure standardized and reliable mineral identification. The spectral library included representative alteration and host-rock minerals, including almandine, alunite, calcite, dolomite, epidote, goethite, hematite, illite, kaolinite, and quartz. The Spectral Angle Mapper algorithm measures the spectral similarity between image spectra and reference endmembers by calculating the spectral angle in multidimensional feature space, making it relatively insensitive to illumination effects while preserving spectral shape [41]. Since no universal threshold exists for SAM classification, angular thresholds were evaluated through iterative testing, and a range of 0.10-0.15 radians was selected because it provided the best compromise between omission and commission errors and showed the highest agreement with geological maps, mining lease boundaries, and field observations. Similar threshold optimization approaches have been widely adopted in mineral exploration studies using multispectral remote sensing [42,43]. The resulting mineral classification outputs were subsequently validated against known geological formations and mining-related occurrences to assess spatial reliability. The spectral processing workflow and SAM classification integrated spectral methodology enhances the robustness of hydrothermal alteration detection in structurally complex mountainous environments.

Result

Spectral angle mapper (SAM) classification

The Spectral Angle Mapper (SAM) classification was applied to ASTER and Landsat-8 datasets to identify and delineate hydrothermal alteration minerals associated with copper mineralization within District Skardu, Gilgit-Baltistan. SAM is a robust spectral classification technique that compares image spectra with reference mineral spectra derived from established spectral libraries, allowing accurate discrimination of alteration assemblages based on spectral similarity. In this study, reference spectra for alunite, almandine, calcite, dolomite, epidote, goethite, hematite, illite, kaolinite, and quartz were selected from the ASTER and USGS spectral libraries to characterize the mineralogical composition of the study area. The classification results reveal substantial differences between ASTER and Landsat-8 in terms of mineral detection capability and spatial delineation accuracy. Overall, ASTER produced more extensive and spatially coherent mineral distributions, particularly for minerals exhibiting diagnostic absorption features in the Shortwave Infrared (SWIR) region.

The enhanced spectral resolution of ASTER enabled improved discrimination of alteration minerals commonly associated with hydrothermal systems, whereas Landsat-8 provided broader regional patterns with comparatively reduced mineralogical specificity. The spatial distribution of classified minerals demonstrates the occurrence of extensive hydrothermal alteration zones across northern, central, and northeastern sectors of the study area. These alteration zones correspond closely with structurally controlled corridors, fault systems, and lithological contacts that likely served as pathways for mineralizing fluids. The resulting mineral maps provide a valuable basis for evaluating the hydrothermal evolution of the region and identifying areas with elevated mineral exploration potential. The sensor specifications summarized in (Table 3) highlight the complementary characteristics of ASTER and Landsat-8 for mineral exploration applications. ASTER offers superior spectral capability within the SWIR region through dedicated mineral-sensitive bands, enabling detailed identification of alteration minerals. Landsat-8 provides broader spatial coverage and regional geological context, making it useful for reconnaissance-scale investigations. The integration of both datasets therefore supports multi-scale characterization of alteration systems across the Skardu region.

Table 3: Satellite data specifications.

Parameters	ASTER	Landsat-8
Spatial Resolution	15m (VNIR), 30m (SWIR), 90m (TIR)	30m (VNIR/SWIR), 15m (Pan)
Spectral Range (μm)	0.52-11.65	0.43-12.50
Number of Bands	14	11
SWIR Capability	Yes	Yes

Mineral-specific SAM classification

Alunite: Alunite is a characteristic mineral of advanced argillic alteration and is commonly associated with acidic hydrothermal environments related to porphyry and epithermal mineralization systems. Its occurrence serves as an important indicator of hydrothermal fluid activity and potential ore-forming processes. The ASTER-derived SAM classification identified approximately 43.04km^2 of alunite-bearing terrain distributed primarily across the northern and central sectors of the study area. These occurrences correspond closely with structurally controlled zones exhibiting evidence of hydrothermal alteration. The high spectral resolution of ASTER within the critical 2.17-2.20μm absorption region enabled accurate identification of alunite-rich zones and produced continuous, geologically meaningful alteration patterns.

In contrast, Landsat-8 identified only 3.49km^2 of alunite-bearing terrain, represented by isolated and discontinuous patches (Figure 3). The limited detection capability reflects the broader spectral bandwidths of Landsat-8 SWIR channels, which reduce discrimination between alunite and spectrally similar clay minerals. The nearly twelve-fold increase in mapped area obtained from ASTER demonstrates the importance of narrowband SWIR observations for advanced argillic alteration mapping and highlights the potential significance of the identified alunite zones for future exploration activities.

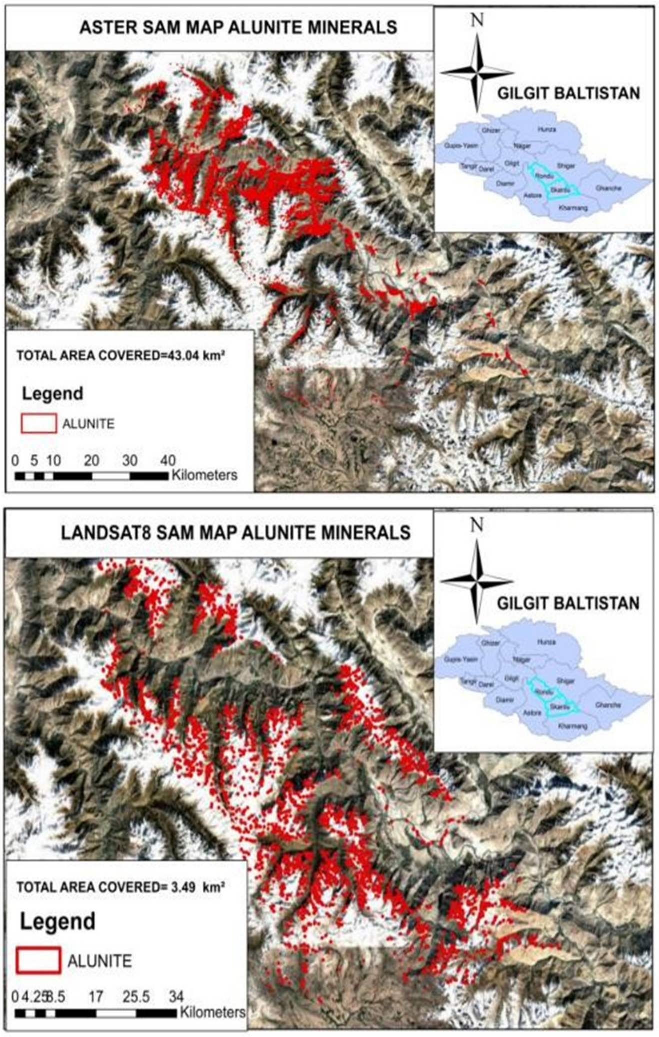

Figure 3: Comparative mapping of alunite mineral distribution using Spectral Angle Mapper (SAM) classification from ASTER and Landsat-8 datasets.

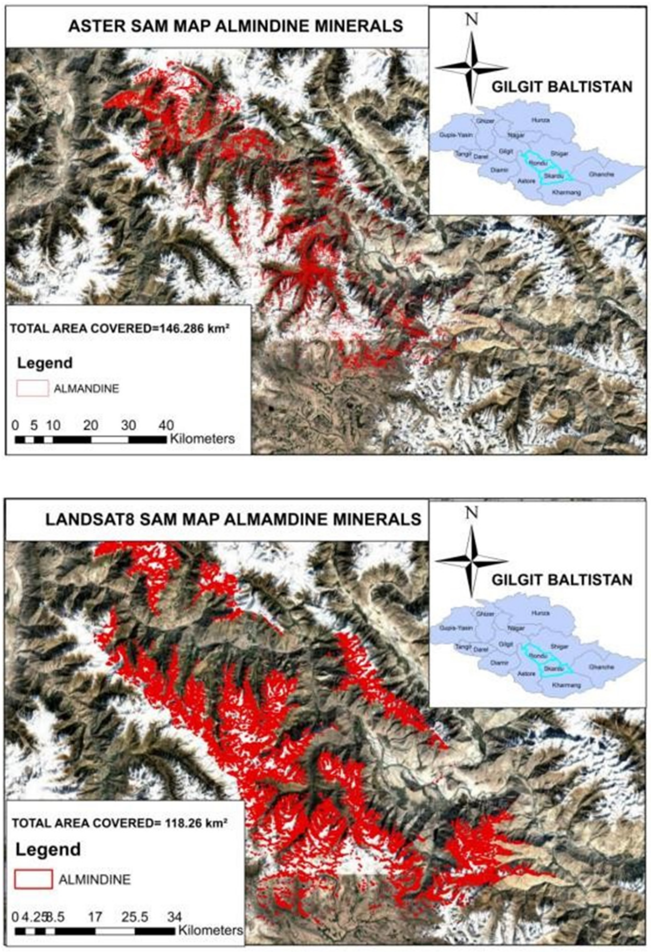

Figure 4: Comparative mapping of almandine mineral distribution using Spectral Angle Mapper (SAM) classification from ASTER and Landsat-8 datasets.

Almandine: Almandine is a metamorphic garnet mineral commonly associated with medium- to high-grade metamorphic environments and provides important information regarding regional lithological variations and metamorphic processes. Although not a direct hydrothermal indicator, its distribution contributes to the geological interpretation of the study area. SAM classification successfully identified almandine-bearing lithologies within the study region (Figure 4). The detected occurrences were primarily associated with metamorphic units exposed throughout structurally uplifted sectors of District Skardu. The mineral distributions coincide with known metamorphic complexes comprising schists and gneisses that characterize the regional geological framework. The identification of almandine demonstrates the capability of spectral classification techniques to distinguish not only hydrothermal alteration minerals but also key lithological indicators. The occurrence of almandine-rich assemblages provides additional geological context for understanding the structural evolution and mineralization controls operating within the study area.

Calcite: Calcite is a major carbonate mineral commonly associated with hydrothermal alteration, skarn systems, and carbonate host rocks. Mapping calcite distributions therefore provides valuable information regarding fluid-rock interactions and alteration processes. ASTER-based classification delineated approximately 28.81km^2 of calcite-bearing terrain concentrated mainly within northern and northwestern sectors of the study area (Figure 5). The mapped zones appear as coherent and continuous bodies corresponding with lithological contacts and structurally controlled carbonate-bearing formations. ASTER's narrow SWIR channels effectively resolved calcite absorption features near 2.33μm, resulting in reliable mineral discrimination. Conversely, Landsat-8 identified only 2.49km^2 of calcite-rich terrain, characterized by scattered and fragmented occurrences. The substantial discrepancy between sensors reflects the limitations of broader spectral bands for resolving subtle carbonate absorption features. The results demonstrate that ASTER provides a more reliable framework for carbonate alteration mapping and may significantly improve exploration targeting within carbonate-hosted mineralization environments.

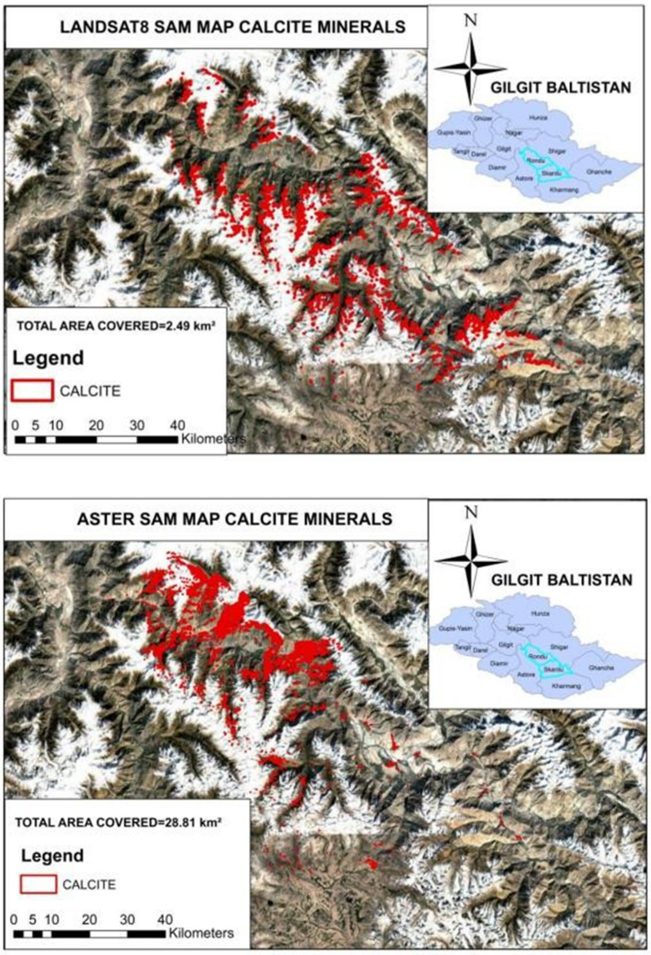

Figure 5: Comparative mapping of calcite mineral distribution using Spectral Angle Mapper (SAM) classification from ASTER and Landsat-8 datasets.

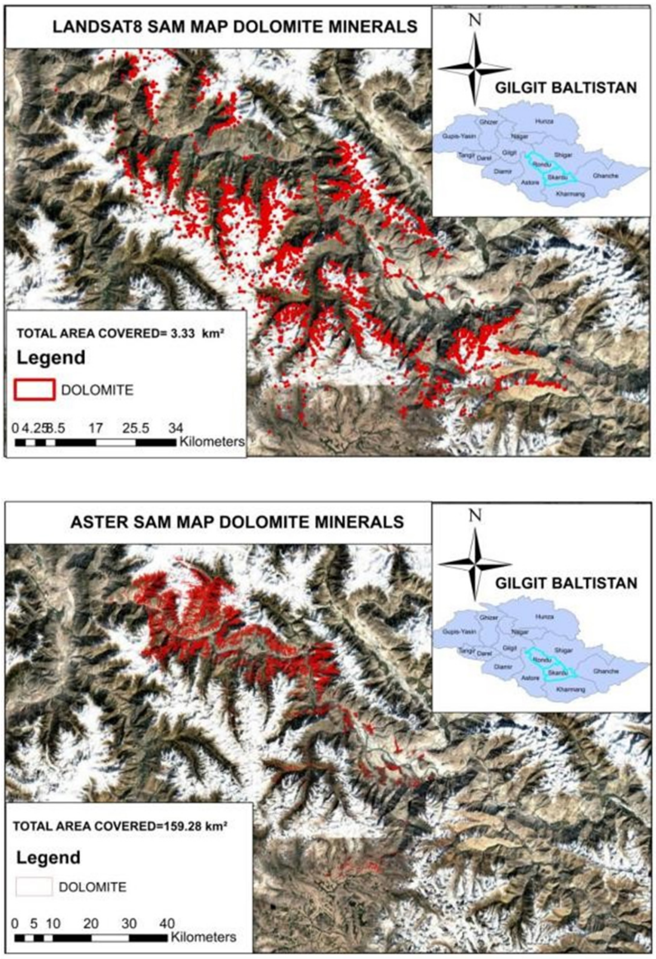

Figure 6: Comparative mapping of dolomite mineral distribution using Spectral Angle Mapper (SAM) classification.

Dolomite: Dolomite represents another important carbonate mineral frequently associated with hydrothermal systems and carbonate replacement processes. Accurate delineation of dolomite-bearing lithologies is critical for understanding fluid pathways and mineralization controls. ASTER mapped approximately 159.28km^2 of dolomite-rich terrain, making it one of the most extensive mineral classes identified in the study. The mapped occurrences form large, continuous bodies distributed predominantly throughout northern and northeastern sectors. These extensive carbonate domains suggest widespread fluid-rock interaction and significant alteration development within the regional geological framework. In contrast, Landsat-8 detected only 3.30km^2 of dolomite-bearing terrain (Figure 6). This nearly fifty-fold difference underscores the importance of ASTER's enhanced SWIR spectral resolution for carbonate mineral discrimination. The results suggest that ASTER-derived dolomite maps provide a more realistic representation of carbonate alteration patterns and contribute significantly to regional mineral exploration assessments.

Epidote: Epidote is commonly associated with propylitic alteration and represents an important indicator of hydrothermal activity surrounding mineralized systems. Its occurrence frequently marks peripheral alteration zones associated with porphyry copper deposits. ASTER-based classification identified approximately 176.86km^2 of epidote-bearing terrain distributed across northern and central sectors of the study area. The mineral exhibits extensive spatial continuity and occurs in association with structurally controlled alteration corridors. The distribution pattern suggests widespread propylitic alteration linked to hydrothermal fluid circulation. Landsat-8 identified 42.01km^2 of epidote-bearing terrain (Figure 7). Although substantial epidote occurrences were detected, the mapped zones appear more fragmented and less coherent than those derived from ASTER. These results confirm ASTER's superior ability to delineate alteration zoning and hydrothermal mineral assemblages within complex mountainous terrains.

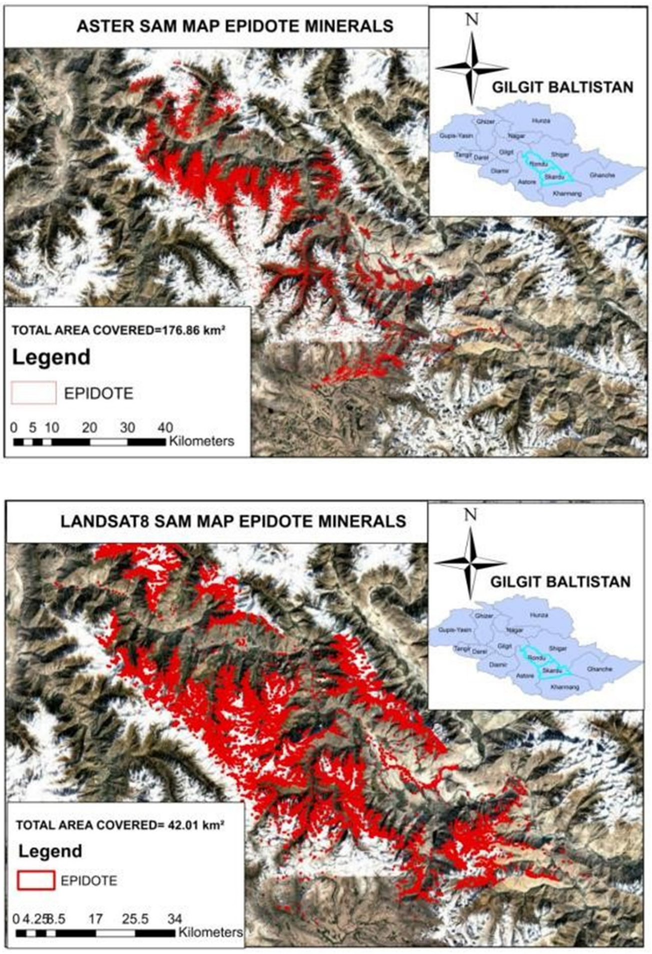

Figure 7: Comparative mapping of epidote mineral distribution using Spectral Angle Mapper (SAM) classification from ASTER and Landsat-8 datasets in District Skardu.

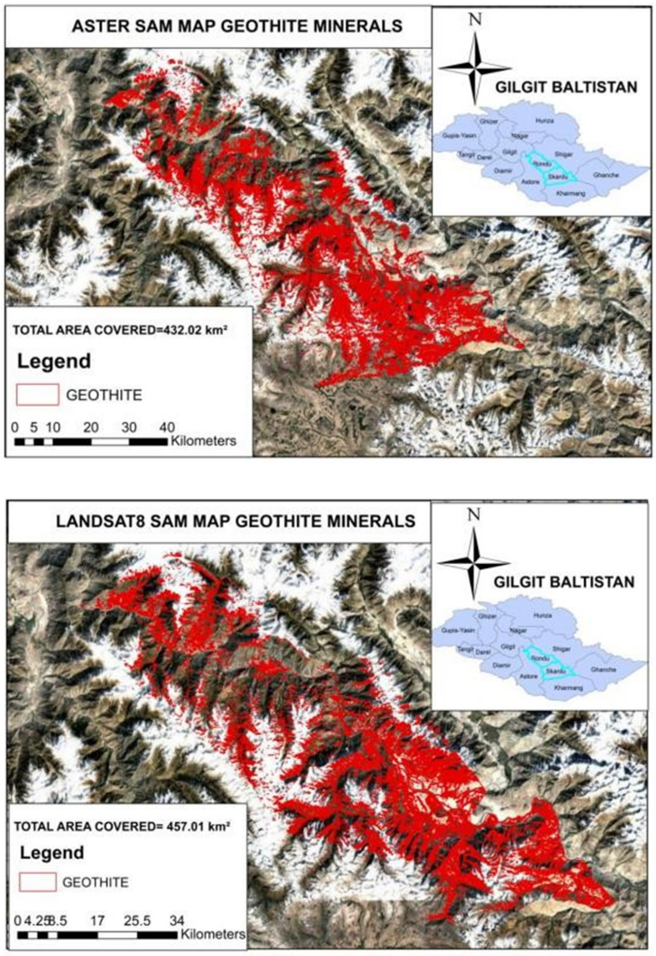

Figure 8: Comparative SAM-based goethite mineral distribution derived from ASTER and Landsat-8 datasets in District Skardu.

Goethite: Goethite is an iron oxyhydroxide mineral commonly associated with weathering processes and hydrothermal iron enrichment. Its occurrence often indicates oxidation of sulfide-bearing mineral systems and therefore represents an important exploration target. ASTER mapped approximately 432.02km^2 of goethite-bearing terrain, making it the most extensive alteration mineral identified in the study area. Significant concentrations occur within central and southern sectors where iron-rich alteration appears particularly intense. The mapped distributions correspond closely with exposed bedrock and structurally controlled alteration systems. Landsat-8 identified approximately 457.01km^2 of goethite-rich terrain (Figure 8). Although the total mapped area slightly exceeds that of ASTER, the Landsat-derived distributions appear more generalized and exhibit lower spatial precision. The broader spectral bandwidths of Landsat-8 likely contributed to spectral mixing and possible overestimation of iron-rich zones. Consequently, ASTER provides more reliable delineation despite the comparable areal coverage.

Hematite: Hematite is a diagnostic iron oxide mineral frequently associated with hydrothermal alteration and oxidized mineral deposits. Its identification is particularly important for exploration targeting due to its close association with mineralized systems. ASTER-based classification delineated approximately 244.11km^2 of hematite-bearing terrain distributed throughout central, northern, and southeastern sectors. The mineral occurs as extensive, well-defined alteration zones associated with exposed bedrock and structurally controlled mineralized corridors. By comparison, Landsat-8 identified 120.19km^2 of hematite-rich terrain (Figure 9). The reduced extent and fragmented nature of the mapped occurrences indicate lower spectral discrimination capability. ASTER's superior performance demonstrates the value of high-resolution VNIR and SWIR observations for accurate iron oxide mapping within hydrothermally altered terrains.

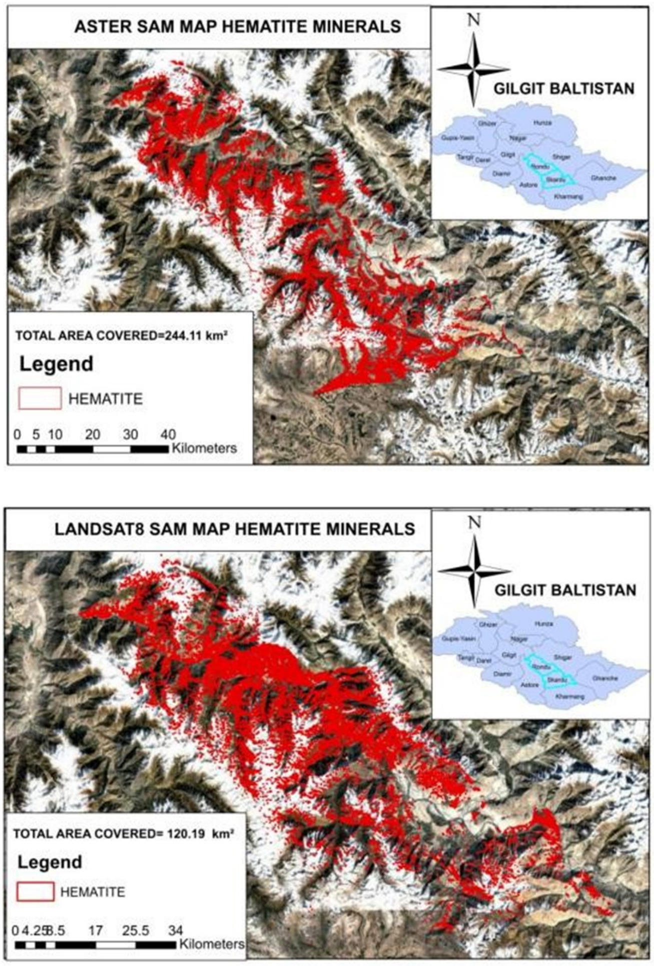

Figure 9: Comparative SAM-based hematite mineral distribution derived from ASTER and Landsat-8 datasets in District Skardu.

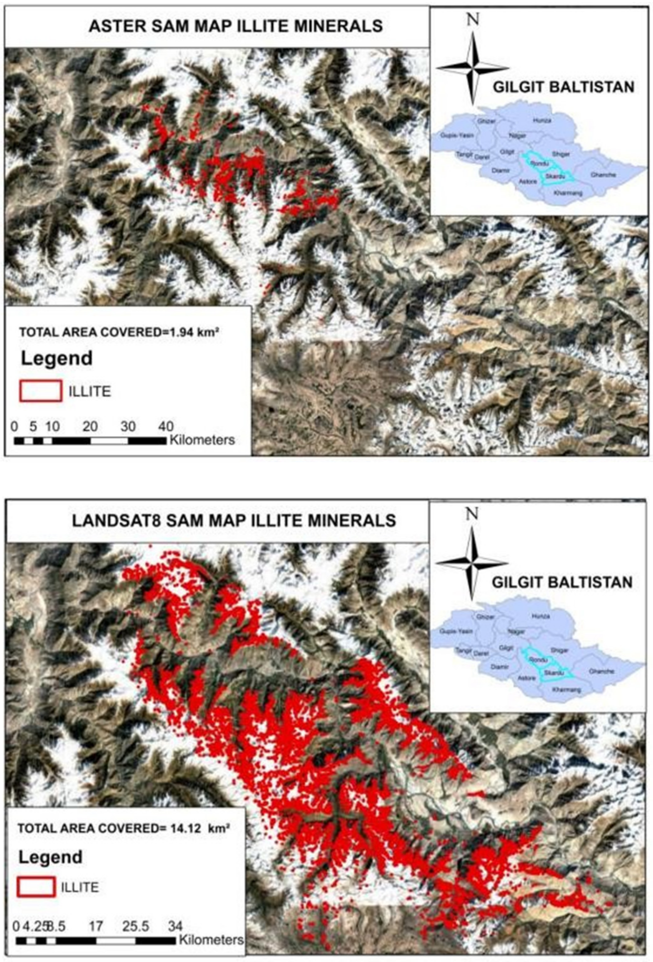

Figure 10: Comparative SAM-based illite mineral distribution derived from ASTER and Landsat-8 datasets in District Skardu.

Illite: Illite is a common phyllosilicate mineral associated with phyllic alteration and hydrothermal fluid-rock interaction. Its occurrence often provides valuable information regarding alteration intensity and hydrothermal zonation. ASTER identified only 1.94km² of illite-bearing terrain, concentrated within localized northern sectors of the study area. The limited extent may reflect restricted surface exposure or spectral interference resulting from complex lithological conditions. In contrast, Landsat-8 mapped approximately 14.12km² of illite-rich terrain distributed more broadly throughout central and southeastern sectors (Figure 10). While the larger area suggests enhanced detection capability, the possibility of spectral confusion with other clay minerals cannot be excluded. Consequently, ASTER likely provides a more conservative and mineralogically reliable representation of illite occurrence.

Kaolinite: Kaolinite is a characteristic clay mineral associated with argillic alteration and hydrothermal systems. Its occurrence serves as a key indicator of mineralizing fluid activity and alteration intensity. ASTER-based classification identified approximately 51.84km² of kaolinite-bearing terrain concentrated primarily within northern sectors of the study area. The mapped zones coincide with hydrothermal alteration corridors and areas of intense weathering. Landsat-8 identified only 2.46km² of kaolinite-rich terrain (Figure 11). The significant difference between sensors reflects ASTER's enhanced capability for resolving kaolinite absorption features within the SWIR region. These findings highlight the importance of ASTER for mapping clay-rich hydrothermal alteration systems and identifying prospective exploration targets.

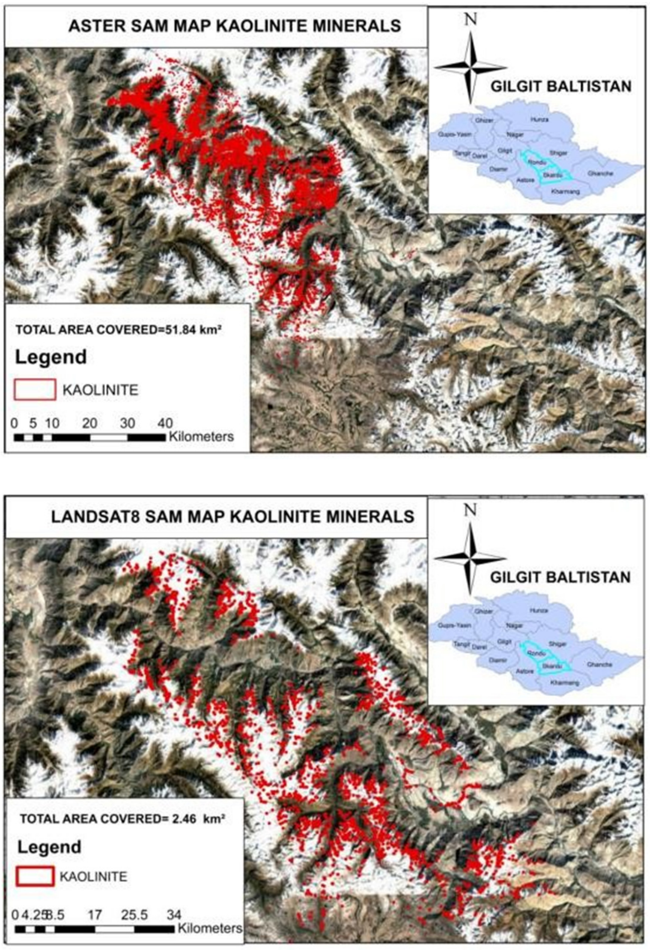

Figure 11: Comparative SAM-based illite mineral distribution derived from ASTER and Landsat-8 datasets in District Skardu.

Quartz: Quartz-rich zones represent silicification processes commonly associated with hydrothermal mineralization. Mapping quartz distributions is therefore essential for identifying structurally controlled fluid pathways and alteration systems.

ASTER delineated approximately 77.17km² of quartz-bearing terrain distributed throughout northern and central sectors. The mapped zones coincide with exposed silica-rich lithologies and structurally controlled mineralized corridors. Landsat-8 identified 23.09km² of quartz-rich terrain (Figure 12). Although major silicified zones were successfully detected, the extent and spatial continuity were significantly lower than those obtained from ASTER. The results confirm ASTER's superior ability to identify subtle silica enrichment and delineate hydrothermal silicification patterns.

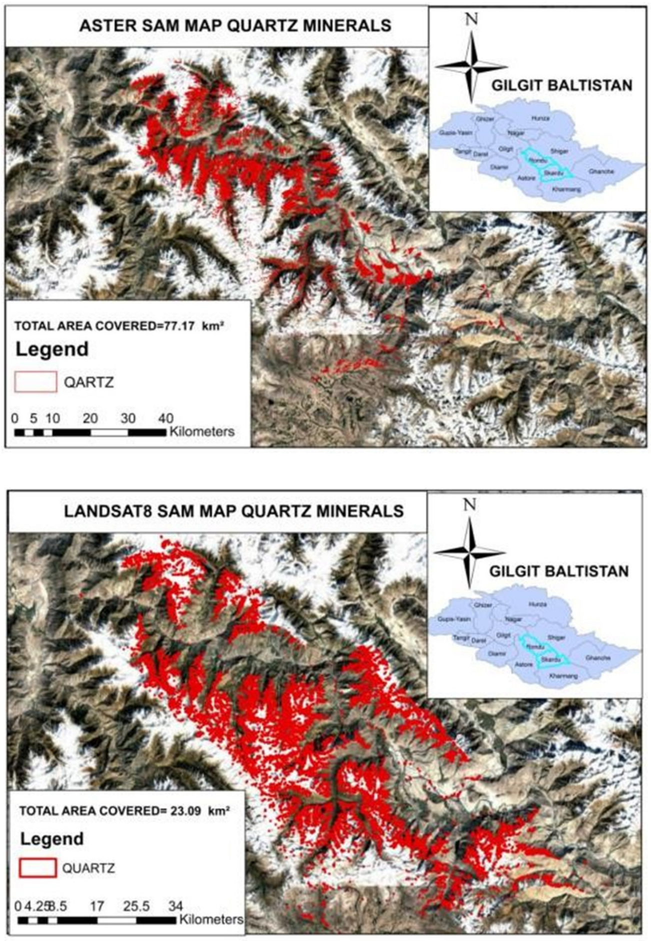

Figure 12: Comparative SAM-based illite mineral distribution derived from ASTER and Landsat-8 datasets in District Skardu.

Comparative Analysis of ASTER and Landsat-8 Mineral Mapping

The comparative Spectral Angle Mapper (SAM) classification results (Figure 13) demonstrate distinct variations in hydrothermal alteration mineral distribution derived from ASTER and Landsat-8 datasets in District Skardu. The mapped mineral assemblages include quartz, hematite, goethite, kaolinite, illite, alunite, epidote, calcite, and dolomite, which collectively represent key indicators of porphyry-related hydrothermal systems. ASTER-derived SAM outputs exhibit sharply defined and spatially coherent mineral zones, reflecting its Superior Shortwave Infrared (SWIR) spectral resolution. In contrast, Landsat-8 results display broader, more generalized mineral distributions with reduced boundary precision and increased spectral overlap. This contrast highlights ASTER's enhanced capability for detailed mineral discrimination, whereas Landsat-8 provides broader reconnaissance-scale geological context. Quartz-rich zones, iron oxides (hematite and goethite), and clay minerals (kaolinite and illite) are distinctly mapped in ASTER data, whereas Landsat-8 tends to amalgamate these lithologies into less distinct spectral classes. Consequently, ASTER is more suitable for detailed exploration targeting, while Landsat-8 supports regional alteration trend identification.

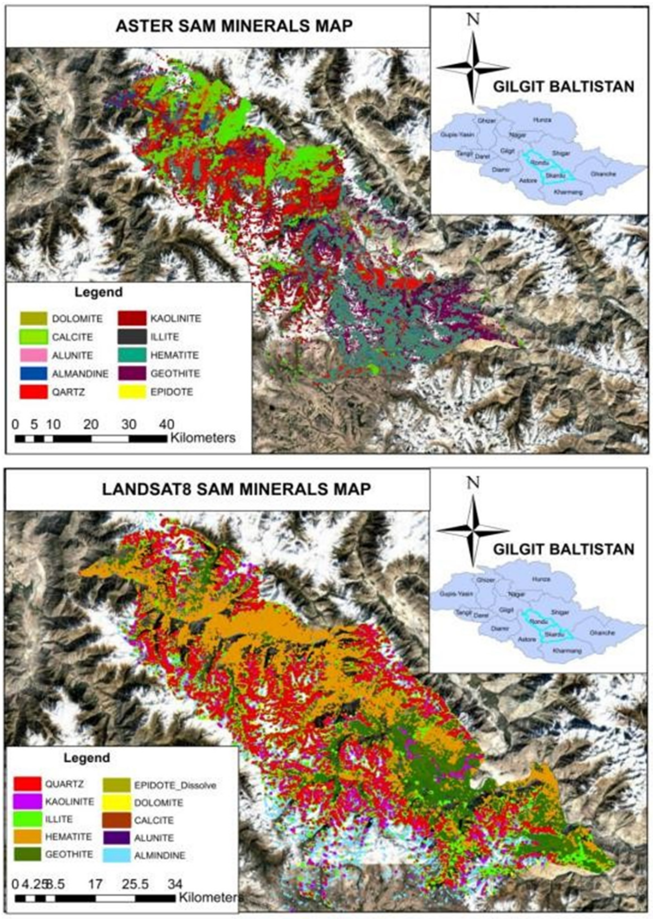

Figure 13: Integrated SAM-based mineral classification maps derived from ASTER and Landsat-8 datasets showing spatial distribution of hydrothermal alteration assemblages in District Skardu.

The spectral characteristics summarized in (Table 4) indicate that ASTER's extended SWIR coverage enables detection of a wider range of alteration minerals, particularly carbonates, clays, and aluminosilicates. Landsat-8, although limited in spectral specificity, effectively captures iron-oxide and some clay-related signatures. Overlapping absorption features in the 2.0-2.4μm range are better resolved by ASTER, confirming its superiority for mineralogical discrimination in complex terrains.

Table 4: Diagnostic spectral absorption features of alteration minerals.

Mineral	Diagnostic Absorption Features (μm)	Detected by Sensor
Kaolinite	2.20-2.30	ASTER
Illite	2.20-2.40	ASTER, Landsat-8
Hematite	0.86-0.90, 2.20	ASTER, Landsat-8
Alunite	2.17-2.20	ASTER
Dolomite	2.31-2.35	ASTER
Calcite	2.33-2.35	ASTER
Quartz	2.21-2.25 (weak feature)	ASTER
Goethite	0.90-1.00, 2.27	ASTER, Landsat-8
Epidote	2.20-2.30	ASTER
Almandine	1.80-2.00	ASTER

The comparative bar chart (Figure 14) illustrates significant variations in mapped mineral extents between ASTER and Landsat-8 datasets. Across most mineral classes, ASTER consistently reports higher or more refined area estimates, indicating improved spectral sensitivity and classification accuracy. Landsat-8, while effective for broad identification, tends to underestimate or generalize mineral extents due to its relatively lower spectral resolution. Table 5 demonstrates that ASTER provides significantly improved mineral discrimination across key alteration minerals. Alunite and quartz show particularly strong spectral definition in ASTER outputs, while Landsat-8 fails to consistently resolve their spatial continuity. Goethite is detected by both sensors; however, ASTER provides more spatially reliable and geologically consistent mapping.

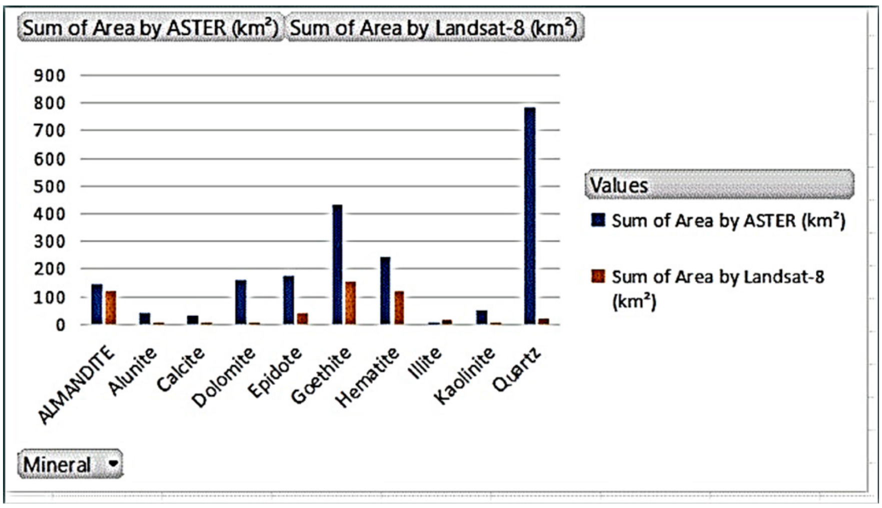

Figure 14: Comparative analysis of mineral mapping areas derived from ASTER and Landsat-8 SAM classification results across key alteration minerals in District Skardu.

Table 5: SAM classification performance comparison.

Mineral	ASTER Classification Result	Landsat-8 Classification Result	Interpretation
Alunite	Clearly and continuously mapped	Sparsely and discontinuously detected	ASTER superior
Quartz	Moderately to well-defined zones	Weak and fragmented signatures	ASTER superior
Goethite	Well-defined and spatially coherent	Broad but less distinct distribution	Slight ASTER advantage

Table 6: Sensor-based capability comparison.

Parameter	ASTER	Landsat-8
Spectral Resolution	High (SWIR-optimized)	Moderate
Mineral Differentiation	High precision	Generalized
Spatial Coverage	Moderate	Extensive
Suitability for Mapping	Detailed exploration targeting	Regional reconnaissance

Table 6 summarizes the fundamental sensor differences influencing mineral mapping performance. ASTER's SWIR-optimized spectral configuration enables high-precision mineral discrimination, making it suitable for detailed exploration. In contrast, Landsat-8 provides broader spatial coverage and is more effective for regional-scale reconnaissance and preliminary geological assessment.

Band-ratio index analysis

This section presents the results derived from band ratio indices designed to enhance the detection of key hydrothermal alteration minerals, specifically quartz, carbonates, and clay minerals, using ASTER and Sentinel-2A multispectral datasets. These indices are fundamental in identifying alteration zones commonly associated with porphyry and epithermal mineral systems. Both sensors provide relevant spectral information in the Shortwave Infrared (SWIR) region; however, they differ significantly in spectral resolution and band configuration, which influences mineral discrimination capability. Band ratio techniques were applied to enhance diagnostic absorption features and suppress background lithological noise, thereby improving the interpretability of large multispectral datasets. Quartz indices were used to delineate silica-enriched zones, carbonate indices targeted calcite- and dolomite-bearing lithologies, and clay indices highlighted hydroxyl-bearing phyllosilicates such as kaolinite, illite, and alunite. ASTER, with its six SWIR bands (2.1-2.5μm), provides enhanced spectral sensitivity for distinguishing closely related mineral phases. In contrast, Sentinel-2A, with only two SWIR bands, offers improved spatial resolution (20m) and revisit frequency, making it suitable for regional reconnaissance and temporal monitoring when integrated with ASTER data. Table 7 summarizes the band ratio configurations used for mapping hydrothermal alteration minerals across both Sentinel-2A and ASTER datasets. Sentinel-2A indices utilize SWIR bands B11 and B12 to differentiate quartz, carbonates, and clay-rich zones, while ASTER indices leverage its narrower and more mineral-sensitive SWIR bands for enhanced spectral separation. The ASTER clay index, in particular, exploits internal band relationships to emphasize hydroxyl-bearing mineral responses, improving discrimination in structurally complex terrains.

Table 7: Band ratio indices used for mineral mapping (ASTER and Sentinel-2A).

Index Type	Sentinel-2A Formula	ASTER Formula	Target Minerals
Quartz Index	B11/B12	B14/B12	Quartz
Clay Index	B5/B6	$(B5 \times B6)/B6^2$	Kaolinite, Illite, Alunite
Carbonate Index	B13/B14	B13/B14	Calcite, Dolomite

Table 8: Sentinel-2A band configuration for mineral indices.

Index Type	Band Formula (Sentinel-2A)	Wavelength Range (μm)	Spectral Sensitivity
Quartz Index	B11/B12	1.61/2.19	Silica-rich lithologies
Carbonate Index	B12/B11	2.19/1.61	Calcite, Dolomite
Clay Index	(B11+B12)/2	SWIR mean response	Kaolinite, Illite, Alunite

Table 8 illustrates the Sentinel-2A band ratio framework used to extract hydrothermal alteration signatures. The Quartz Index enhances silica-rich outcrops by exploiting reflectance contrast between B11 and B12, while the inverse carbonate ratio emphasizes carbonate-bearing lithologies. The clay index, derived as the mean of SWIR bands, provides a generalized measure of hydroxyl-bearing mineral abundance. Although Sentinel-2A lacks the spectral resolution of ASTER, its fine spatial resolution enables effective mapping of broad alteration trends, especially when integrated with higher spectral resolution datasets. The combined use of ASTER and Sentinel-2A band ratio indices enable a multi-scale mineral mapping strategy, where ASTER provides high spectral discrimination of alteration mineralogy, while Sentinel-2A contributes high spatial detail for structural and regional mapping. This integration significantly improves the reliability of hydrothermal alteration mapping in the complex geological terrain of District Skardu.

Carbonate index

Carbonate index mapping identified extensive carbonate-bearing zones associated with calcite and dolomite-rich lithologies. Sentinel-2A delineated approximately 31.19km^2 of carbonate-rich terrain, while ASTER identified 28.35km^2 (Figure 15). Although the mapped areas were similar, ASTER produced more continuous and geologically coherent carbonate distributions. The enhanced spectral sensitivity of ASTER within carbonate absorption regions enabled improved discrimination of carbonate-bearing lithologies and hydrothermal alteration zones.

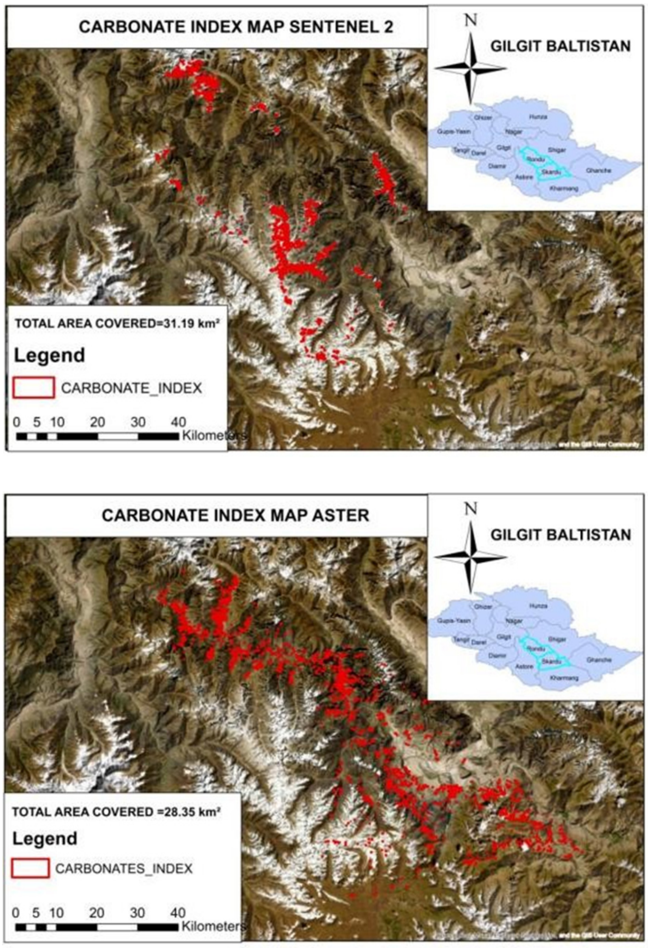

Figure 15: Carbonate index maps derived from Sentinel-2A and ASTER datasets showing spatial distribution of carbonate-rich zones in District Skardu.

Clay index

Clay index analysis revealed widespread distribution of hydroxyl-bearing minerals across the study area. Sentinel-2A mapped approximately 82.08km^2 of clay-rich terrain, significantly exceeding ASTER's 23.20km^2 (Figure 16). The larger mapped extent obtained from Sentinel-2A reflects its finer spatial resolution and enhanced capability for detecting dispersed clay-rich surfaces. However, ASTER provides greater mineralogical specificity and remains essential for distinguishing among clay mineral assemblages.

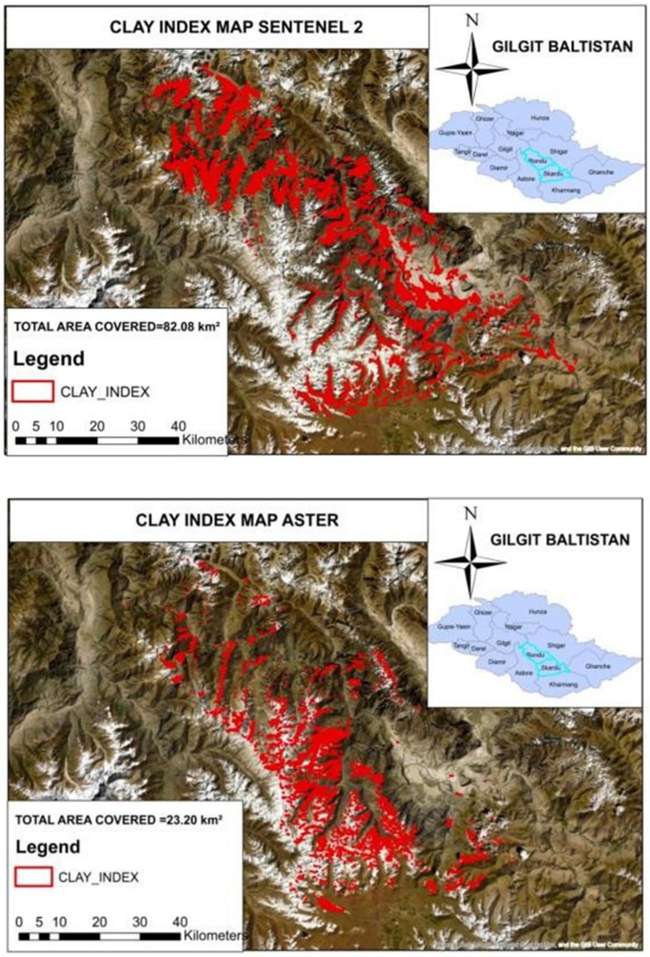

Figure 16: Clay index maps derived from Sentinel-2A and ASTER datasets showing spatial distribution of clay-rich alteration zones in District Skardu.

Quartz index

The quartz index maps derived from Sentinel-2A and ASTER datasets reveal distinct spatial patterns of silica enrichment across District Skardu (Figure 17). Sentinel-2A delineates moderately continuous quartz-rich zones (highlighted in red) along major structural trends in the northern and central sectors. This pattern reflects the sensor's relatively high spatial resolution (20m), which enables effective identification of exposed silicified outcrops and structurally controlled alteration zones.

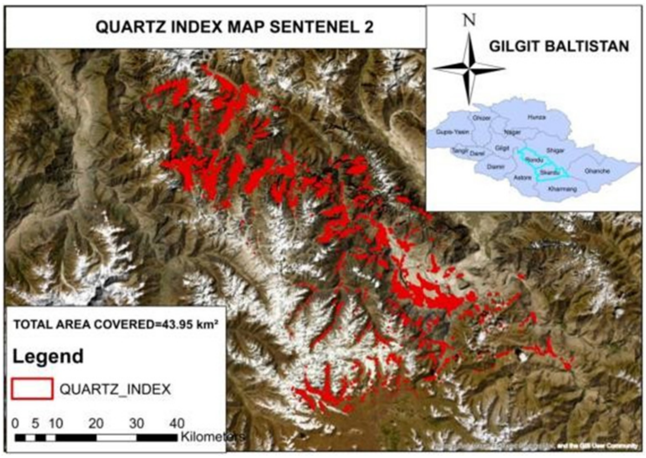

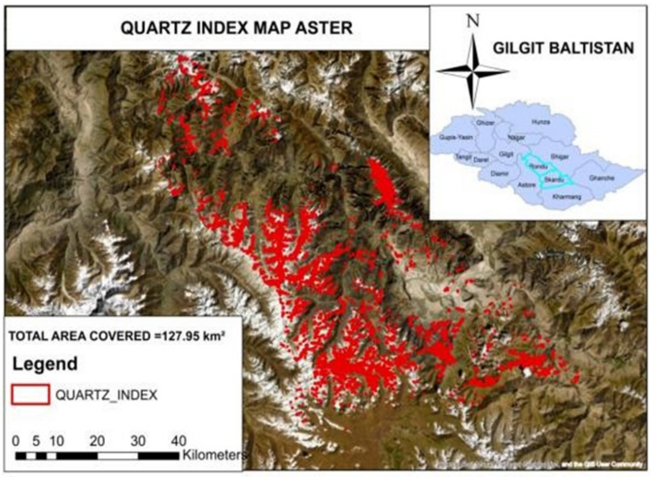

Figure 17: Quartz index maps derived from Sentinel-2A and ASTER datasets showing spatial distribution of silica-rich zones in District Skardu.

In contrast, the ASTER-derived quartz index shows a more extensive and spatially dispersed distribution of silica-rich signatures, particularly across the southern and southeastern regions. This broader detection is attributed to ASTER's Superior Shortwave Infrared (SWIR) spectral resolution, which enhances sensitivity to diagnostic silicate absorption features and enables detection of both strong and subtle quartz-related spectral responses. While ASTER is more effective in capturing low-contrast and alteration-proximal quartz occurrences, Sentinel-2A remains reliable for mapping prominent silicified bodies with higher spatial continuity and more frequent temporal coverage.

Table 9 demonstrates clear variability in mineral detection performance between ASTER and Sentinel-2A datasets. ASTER significantly outperforms Sentinel-2A in quartz detection, mapping 127.95km^2 compared to 43.95km^2, highlighting its enhanced SWIR spectral discrimination of silicate-rich lithologies. Conversely, Sentinel-2A identifies a substantially larger clay-rich area (82.08km^2) compared to ASTER (23.20km^2), reflecting its finer spatial resolution and improved sensitivity to widespread phyllosilicate distributions. Carbonate mapping shows close agreement between both sensors, with Sentinel-2A (31.19km^2) and ASTER (28.35km^2) yielding comparable extents, indicating similar effectiveness in detecting calcite- and dolomite-bearing lithologies despite differing spectral configurations.

Table 9: Area coverage of mineral indices derived from ASTER and Sentinel-2A.

Mineral Index	Sentinel-2A Area (km^2)	ASTER Area (km^2)
Quartz Index	43.95	127.95
Clay Index	82.08	23.2
Carbonate Index	31.19	28.35

Figure 18 presents a comparative evaluation of mineral index-based area coverage derived from ASTER and Sentinel-2A datasets. The results indicate clear differences in detection capability across the three mineral indices: carbonate, clay, and quartz. For the carbonate index, both sensors demonstrate closely aligned performance, with Sentinel-2A mapping approximately 31km^2 and ASTER mapping around 28km^2, indicating consistent carbonate detection capability. In the clay index, Sentinel-2A significantly outperforms ASTER by delineating approximately 82km^2 compared to 23km^2, reflecting its superior spatial resolution and ability to capture widespread phyllosilicate alteration zones. In contrast, the quartz index shows a strong advantage for ASTER, which maps approximately 127km^2 compared to 43km^2 for Sentinel-2A, confirming ASTER's higher spectral sensitivity to silicate mineral absorption features in the SWIR region.

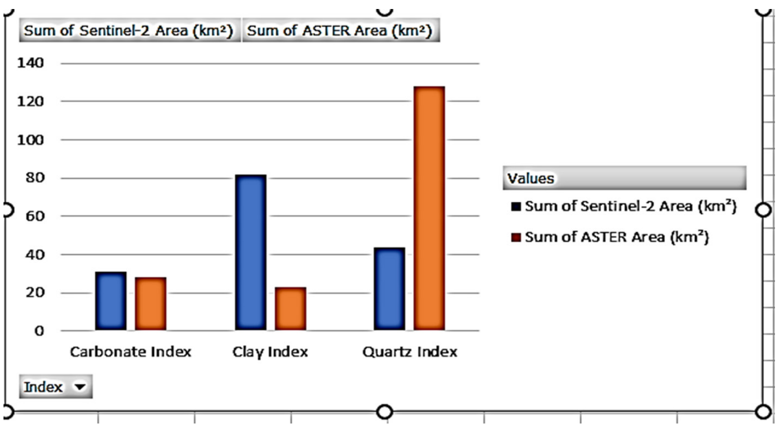

Figure 18: Comparative bar chart showing mineral index-based area coverage (km²) derived from Sentinel-2A and ASTER datasets for quartz, clay, and carbonate minerals.

Composite alteration mapping

Integration of quartz, clay, and carbonate indices generated composite alteration maps that provide a comprehensive representation of hydrothermal processes across District Skardu. The composite maps reveal strong spatial associations between multiple alteration assemblages and major structural features, suggesting that fault systems played a critical role in controlling hydrothermal fluid movement. ASTER-derived composite maps exhibit superior mineralogical discrimination and define alteration corridors with greater clarity. Sentinel-2A, however, provides enhanced spatial detail that facilitates identification of smaller alteration features and structural lineaments. The combined use of both datasets therefore offers a robust framework for regional mineral exploration and target generation.

Ground truth validation

Ground truth validation was conducted using the active mining lease operated by Shahzad International Pvt. Ltd. within Shigri Balla, District Skardu. The lease area provided an independent reference for assessing the reliability of remote sensing-derived mineral maps and alteration models. Overlay analysis demonstrated strong spatial correspondence between mapped alteration zones and known mineralized areas within the lease boundary (Figure 19). Quartz, clay, carbonate, hematite, kaolinite, and alunite anomalies identified through SAM classification and band-ratio analysis consistently coincided with documented mineral occurrences and active mining operations.

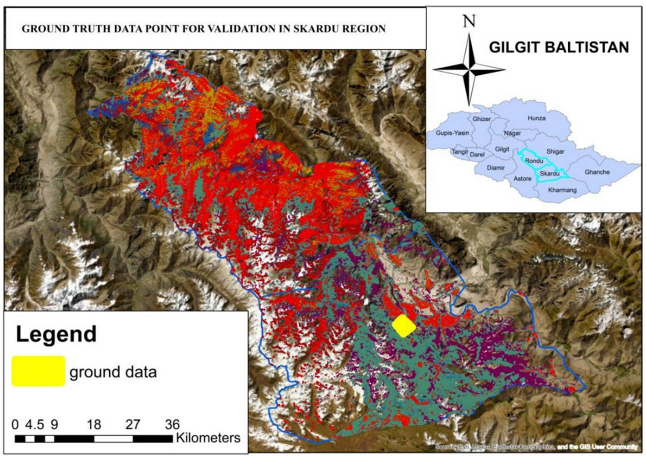

Figure 19: Ground-truth validation map showing overlay of SAM-based mineral classification results with the Shahzad International Pvt. Ltd. lease boundary in Shigri Balla, District Skardu.

Field observations further confirmed the presence of hydrothermal alteration, quartz veining, and visible copper staining within the validated area. The agreement between remotely sensed alteration signatures and field evidence demonstrates the effectiveness of the integrated ASTER, Sentinel-2A, and Landsat-8 approach for mineral exploration in mountainous and inaccessible terrains. These findings provide strong support for the application of multi-sensor remote sensing techniques in identifying copper-associated hydrothermal systems within the Karakoram region. Although the mapped hydrothermal alteration zones showed strong spatial agreement with mining lease boundaries, regional geological maps, and GPS-referenced field observations, a comprehensive quantitative accuracy assessment, including Overall Accuracy (OA), Producer's Accuracy (PA), User's Accuracy (UA), and the Kappa coefficient, could not be performed because of the limited availability of extensive ground-truth mineralogical observations in the rugged mountainous terrain of the study area. Nevertheless, the consistent correspondence between the remotely sensed alteration patterns and independently verified geological evidence demonstrates the reliability of the proposed multi-sensor framework for regional hydrothermal alteration mapping and copper prospectivity assessment. Future studies should incorporate additional field sampling, laboratory-confirmed mineralogical analyses, and statistical accuracy assessment to further validate and refine the proposed methodology.

Discussion

The integration of ASTER, Landsat-8, and Sentinel-2A datasets provided valuable insights into the spatial distribution of hydrothermal alteration minerals associated with potential copper mineralization in District Skardu. The results demonstrate that sensor selection substantially influences the detection and delineation of alteration assemblages due to differences in spectral and spatial resolution. Among the evaluated datasets, ASTER consistently exhibited superior performance for mineral discrimination, particularly for hydroxyl-bearing, carbonate, and silica-rich minerals, owing to its dedicated Shortwave Infrared (SWIR) bands. These findings confirm the importance of high spectral resolution in hydrothermal alteration mapping and are consistent with previous investigations that identified ASTER as one of the most effective multispectral sensors for mineral exploration in arid and mountainous terrains. Similar observations have been reported in hydrothermal alteration studies conducted in the Zagros Mountains (Iran), the Tibetan Plateau (China), and the Arabian Shield, where ASTER consistently outperformed Landsat-based sensors because of its six SWIR bands specifically designed for mineral discrimination [44-46]. These studies demonstrated that ASTER effectively distinguishes hydroxyl-bearing, carbonate, and silica-rich alteration minerals associated with porphyry copper systems, supporting the findings obtained for the Karakoram region in the present study.

The Spectral Angle Mapper (SAM) classification results revealed significant differences between ASTER and Landsat-8 in the detection of key alteration minerals. ASTER successfully mapped substantially larger and more coherent occurrences of alunite, kaolinite, quartz, dolomite, epidote, and hematite compared with Landsat-8. For example, ASTER identified 43.04km^2 of alunite-bearing terrain, whereas Landsat-8 detected only 3.49km^2. Similarly, dolomite occupied 159.28km^2 in the ASTER classification but only 3.30km^2 in the Landsat-8 results. These differences can be attributed to ASTER's narrow SWIR channels, which capture diagnostic absorption features between 2.0 and 2.5μm, a critical spectral region for distinguishing hydrothermal alteration minerals. In contrast, the broader SWIR bands of Landsat-8 reduce spectral separability and increase the likelihood of mixed-pixel effects, particularly in rugged mountainous environments where lithological heterogeneity is pronounced. Comparable results have been reported by Pour & Hashim (2015), who demonstrated that ASTER provided significantly higher hydrothermal mineral discrimination than Landsat imagery in structurally complex terrains due to its enhanced SWIR spectral resolution.

Likewise, Rowan & Mars [31] concluded that ASTER improves identification of alteration assemblages associated with porphyry mineralization, particularly where mixed-pixel effects limit the performance of broader multispectral sensors. Quartz, kaolinite, and alunite are commonly associated with silicic and argillic alteration zones developed around hydrothermal systems and porphyry-style mineralization [47,48]. The extensive distribution of these minerals identified by ASTER therefore suggests the presence of significant hydrothermal activity within the study area. Quartz-rich zones mapped by ASTER covered 77.17km^2, compared with only 23.09km^2 identified by Landsat-8. Likewise, ASTER detected more than twenty times the area of kaolinite mapped by Landsat-8. These observations indicate that ASTER is capable of resolving subtle spectral variations associated with alteration halos that are not readily distinguishable in coarser multispectral datasets. The spatial association between quartz, kaolinite, alunite, and structurally controlled zones further supports the interpretation of hydrothermal fluid circulation pathways within the Skardu region. These mineral assemblages are characteristic of porphyry copper systems documented in the Himalayas, Tibetan Plateau, and Central Asian Orogenic Belt, where quartz, kaolinite, and alunite commonly occur within silicic and argillic alteration halos surrounding mineralized intrusions [49,50]. The similarity between the alteration patterns identified in this study and those reported from comparable tectonic environments further strengthens the geological interpretation.

The mapping of iron oxide minerals also provided important information regarding potential mineralized systems. Hematite and goethite are widely recognized indicators of oxidation processes associated with hydrothermal alteration and weathering of sulfide-rich deposits. ASTER mapped 244.11km^2 of hematite-bearing terrain compared with 120.19km^2 identified by Landsat-8, indicating superior discrimination of ferric iron minerals. Interestingly, Landsat-8 produced a slightly larger goethite extent (457.01km^2) than ASTER (432.02km^2). This discrepancy likely reflects spectral mixing and classification generalization caused by Landsat-8's broader spectral bands, which may result in overestimation of iron oxide occurrences. ASTER-derived maps, however, exhibited greater spatial coherence and better correspondence with known geological structures, suggesting higher mineralogical reliability. Band-ratio analysis further highlighted the complementary strengths of ASTER and Sentinel-2A. The quartz index derived from ASTER identified 127.95km^2 of silica-rich terrain, nearly three times the area mapped using Sentinel-2A (43.95km^2). This result reflects ASTER's enhanced sensitivity to silica-related absorption features in the SWIR region. Conversely, Sentinel-2A detected a substantially larger clay-rich area (82.08 km^2) compared with ASTER (23.20km^2). The higher spatial resolution of Sentinel-2A allows more effective recognition of small-scale clay-rich exposures and alteration zones, particularly in areas characterized by fragmented surface expressions. However, the broader spatial distribution observed in Sentinel-2A may also indicate increased sensitivity to mixed spectral responses and therefore requires confirmation using higher spectral resolution datasets such as ASTER. Similar complementary performance between Sentinel-2A and ASTER has recently been reported in multisensor mineral exploration studies, where Sentinel-2A contributed improved spatial delineation of alteration zones while ASTER provided superior mineralogical discrimination through its SWIR bands [50,51]. These findings demonstrate that integrating both sensors provides greater exploration reliability than either dataset alone.

Carbonate index results showed strong agreement between the two sensors, with Sentinel-2A and ASTER mapping 31.19km^2 and 28.35km^2 of carbonate-rich terrain, respectively. Despite the similarity in total area, ASTER generated more continuous and geologically coherent carbonate zones, whereas Sentinel-2A produced more fragmented patterns. This observation emphasizes the complementary relationship between spatial and spectral resolution in alteration mapping. While Sentinel-2A provides enhanced spatial detail, ASTER offers superior mineralogical discrimination that is critical for accurate geological interpretation. The spatial integration of SAM classifications and spectral indices revealed several alteration assemblage's characteristic of hydrothermal mineral systems. Quartz-rich silicification zones commonly coincided with clay and carbonate alteration areas, suggesting the presence of complex hydrothermal processes involving multiple alteration stages. The observed mineral associations are consistent with alteration patterns reported from porphyry copper environments, where silicic, argillic, and carbonate alteration occur in close spatial proximity. The concentration of these alteration assemblages along structural trends and fault-controlled corridors further supports their genetic relationship with hydrothermal fluid migration pathways.

Ground-truth validation provided independent confirmation of the remote sensing results. Overall, the present findings agree well with previous remote sensing investigations conducted in tectonically active mountain belts, confirming that multisensor integration improves the identification of hydrothermal alteration systems compared with single-sensor approaches. The combined use of ASTER, Sentinel-2A, and Landsat-8 enables simultaneous exploitation of high spectral resolution, fine spatial resolution, and regional coverage, thereby providing a more comprehensive interpretation of alteration mineral assemblages than individual datasets alone. The alteration zones identified through ASTER, Sentinel-2A, and Landsat-8 analyses showed strong spatial correspondence with the active mining lease operated by Shahzad International Pvt. Ltd. in Shigri Balla. Elevated quartz, clay, carbonate, hematite, and alunite signatures occurred within and around the lease boundary, while field observations confirmed the presence of hydrothermally altered rocks, quartz veining, and copper-related surface staining. The convergence of multiple mineral indicators within the validated area significantly increases confidence in the interpretation and demonstrates the effectiveness of integrating spectral indices with SAM classification for mineral exploration in inaccessible mountainous regions. Overall, the results indicate that ASTER remains the most effective multispectral dataset for detailed hydrothermal alteration mapping due to its superior SWIR spectral capability. Sentinel-2A provides valuable high-resolution reconnaissance information and enhances spatial interpretation of alteration patterns, while Landsat-8 contributes regional geological context and long-term data continuity. The integration of these complementary datasets therefore offers a robust and cost-effective framework for mineral exploration in structurally complex terrains such as the Karakoram region of northern Pakistan.

Limitations of the Study

Despite the promising performance of the proposed multi-sensor remote sensing framework, several limitations should be acknowledged. First, the study relies on multispectral satellite imagery, which has lower spectral resolution than hyperspectral sensors and therefore limits the discrimination of minerals with similar spectral characteristics, particularly within clay and carbonate alteration assemblages. In addition, the rugged topography, steep slopes, and variable illumination conditions of the Karakoram region may introduce terrain-induced spectral distortions and mixed-pixel effects despite the application of radiometric, atmospheric, and geometric corrections. Furthermore, differences in spatial and spectral resolution among ASTER, Sentinel-2A, and Landsat-8 may influence the consistency of alteration mapping and contribute to uncertainties during multisensor integration. Another limitation relates to the validation of the classification results. Validation was primarily based on mining lease boundaries, regional geological maps, and GPS-referenced field observations because comprehensive laboratory-based mineralogical analyses and extensive ground-truth datasets were unavailable. Consequently, quantitative classification accuracy metrics, such as Overall Accuracy (OA), Producer's Accuracy (PA), User's Accuracy (UA), and the Kappa coefficient, could not be computed. Moreover, seasonal variations, atmospheric conditions during image acquisition, and the availability of field observations may have influenced the detection and interpretation of hydrothermal alteration minerals. Future studies should incorporate hyperspectral imagery, extensive field spectroscopy, geochemical sampling, and quantitative statistical validation to further improve the reliability, reproducibility, and applicability of the proposed framework for mineral exploration in complex mountainous terrains.

Conclusion

This study developed and evaluated an integrated multi-sensor remote sensing framework for mapping copper-associated hydrothermal alteration zones in District Skardu, Gilgit-Baltistan, using ASTER, Sentinel-2A, and Landsat-8 imagery. The combined application of spectral indices and Spectral Angle Mapper (SAM) classification successfully identified hydrothermal alteration minerals, including quartz, kaolinite, alunite, illite, hematite, goethite, calcite, dolomite, and epidote. Among the evaluated datasets, ASTER demonstrated the highest mineral discrimination capability, delineating 244.11km^2 of hematite, 176.86km^2 of epidote, 159.28km^2 of dolomite, 77.17km^2 of quartz, 51.84km^2 of kaolinite, and 43.04km^2 of alunite, whereas Landsat-8 mapped considerably smaller extents for most alteration minerals, including 120.19km^2 of hematite, 23.09km^2 of quartz, 3.49km^2 of alunite, and 3.30km^2 of dolomite. Band-ratio analysis further showed that ASTER detected 127.95km^2 of quartz-rich terrain, compared with 43.95km^2 identified using Sentinel-2A, while Sentinel-2A mapped a larger clay alteration area (82.08km^2) than ASTER (23.20km^2) because of its finer spatial resolution.

Carbonate alteration mapping showed comparable results, with Sentinel-2A and ASTER identifying 31.19km^2 and 28.35km^2, respectively. Ground-truth validation using the Shahzad International Pvt. Ltd. mining lease, regional geological information, and field observations confirmed strong spatial correspondence between the mapped alteration zones and documented hydrothermal mineralization, including quartz veining, hydrothermal alteration, and visible copper staining. The integration of ASTER's superior SWIR spectral capability, Sentinel-2A's high spatial resolution, and Landsat-8's regional geological coverage produced a more comprehensive interpretation of hydrothermal systems than any individual dataset. The proposed framework provides a rapid, cost-effective, and scalable approach for identifying copper prospectivity in rugged mountainous terrains and offers a transferable methodology for mineral exploration in other tectonically active regions worldwide. By integrating complementary multisensor datasets with spectral analysis and geological validation, this study contributes a practical framework for improving exploration efficiency, reducing reconnaissance costs, and supporting sustainable mineral resource assessment.

Future Research Directions

Although the present study successfully demonstrated the effectiveness of multisensor remote sensing for hydrothermal alteration mapping, several opportunities exist to further improve mineral exploration workflows in the Skardu region and similar geological environments. Future investigations should incorporate hyperspectral satellite datasets such as EnMAP and PRISMA, which provide hundreds of contiguous spectral bands and enable direct identification of mineralogical compositions at a much higher level of precision than multispectral sensors. Such datasets could significantly improve discrimination among spectrally similar clay and carbonate minerals. The integration of machine learning and artificial intelligence algorithms, including Random Forest, Support Vector Machine, Extreme Gradient Boosting, and Deep Learning approaches, represents another promising direction. These methods may enhance classification accuracy and reduce spectral confusion in complex mountainous terrains where traditional spectral matching techniques encounter limitations. Future studies should also incorporate detailed field spectroscopy and geochemical analyses to establish quantitative relationships between spectral signatures and mineral concentrations. Portable spectroradiometer measurements collected from validated alteration zones would provide high-quality endmember spectra for improving classification performance and reducing uncertainty.

Furthermore, combining multispectral and hyperspectral data with geophysical datasets such as magnetic, radiometric, induced polarization, and gravity surveys could facilitate the development of integrated mineral prospectivity models. Such multidisciplinary approaches would improve the identification of subsurface mineralization systems and assist in prioritizing exploration targets. Finally, temporal monitoring using long-term satellite archives may provide insights into surface alteration evolution, weathering processes, and anthropogenic mining activities. Time-series analyses could contribute to sustainable resource management and environmental monitoring in active mining districts throughout Gilgit-Baltistan. Beyond mineral exploration, the proposed multisensor framework has the potential to support strategic mineral resource assessment, sustainable mining planning, and evidence-based decision-making in other tectonically active and mineral-rich regions worldwide. The integration of advanced remote sensing technologies with artificial intelligence, field spectroscopy, geochemical investigations, and geophysical exploration is expected to improve exploration efficiency, reduce operational costs, and minimize environmental impacts associated with conventional exploration techniques. Consequently, the methodology presented in this study provides a scalable and transferable framework for future mineral exploration programs and contributes to the broader advancement of sustainable and technology-driven exploration practices.

Funding Statement

This Research is Self-Funded by the Authors.

Author Contributions

Conceptualization, Zakaria Hussain and Zeenat Khan; methodology, Zeenat Khan, Zakaria Hussain and Basir Ali; formal analysis, Zeenat Khan and Basir Ali; investigation, Zeenat Khan, Daud Khan and Basir Ali; validation, Zeenat Khan and Daud Khan; data curation, Zeenat Khan; visualization, Zeenat Khan and Basir Ali; writing-original draft preparation, Zeenat Khan; writing-review and editing, Zakaria Hussain, Basir Ali, Mahin Jamil and Abdullah Ikram; supervision, Zakaria Hussain and Abdullah Ikram. All authors have read and agreed to the published version of the manuscript.

Acknowledgement

The authors would like to express their sincere gratitude to all individuals and departments who contributed to the successful completion of this research. Special thanks are extended to Al-Mussawir Engineers, Shahzad International Pvt. Ltd and Creative Engineering Zone (CEZ) for their technical support and assistance throughout the study. The authors are also highly grateful to S.E. Syed Hussain Shah, Public Health Engineering Department Rawalpindi, for his valuable guidance and support.

References

1. Chunya Z, Huang S, Zhang B, Shen Y, Yalikun Y, et al. (2026) Mineral prospectivity mapping based on remote sensing and machine learning in the Hatu area, China. Minerals 16(2): 144.
2. Wenxin W, He L, Zhao J, He Z, Chen X, et al. (2026) Alteration mineral mapping and thermal anomaly reconstruction based on GF-5 data: A case study of the Ga'erqiong-Galale Cu-Au mining district, Tibet. Ore Geology Reviews 107185.
3. Susanna G (2026) Hyperspectral remote sensing for mine waste characterization and critical mineral exploration.
4. Saraah I, Goswami A, Jallu S, Shaik RU (2026) Mapping of hydrothermal alteration zones linked to volcanogenic-hosted massive sulphide deposits in the betul belt, Madhya Pradesh, India, using prisma hyperspectral imagery. Remote Sensing Applications: Society and Environment 41: 101842.
5. Silmi AA, Nikolas APP, Shafira H, Asti GM (2025) Remote sensing-based analysis of prospectivity epithermal gold mineralization in the sunda arc region of bogor regency.
6. Matthieu T, Ncube L, Thamaga KH (2026) Monitoring the impacts of mining activities on land cover using remote sensing technologies and machine learning in the musonoi copper-cobalt deposit, democratic Republic of Congo. Geocarto International 41(1): 2620330.
7. Semih E, Akbulut M (2026) Remote sensing of listvenite hydrothermal alteration in vezirler mélange, kula (Western Türkiye): Landsat-7 ETM+, crosta-PCA and band-ratio mapping. Türkiye Jeoloji Bülteni pp. 169-188.
8. García JF, Mendoza ME, Leija EG, Búrquez A (2022) Temporal and spatial analysis of hydrothermal alteration zones using multispectral methods and their contribution to understanding territorial dynamics: A review of recent studies.
9. Joy T GC, Dela Cruz AEC, Principe JA, Sarmiento CJS, Queaño KL (2026) Mapping of potential alteration zones for mineralization prospects using remotely sensed data: Case of Mankayan mineral district, Benguet, Philippines. ISPRS Annals 10: 269-276.
10. Lv J, Zi L, Lu C, Tong J, Chang H, et al. (2025) Mining prediction based on coupling structural-alteration anomalies in Tsagaankhairkhan Cu-Au mine, Mongolia using multi-source remote sensing data. Minerals 15(10): 1005.
11. Kalkhoran SE, Seyyed SG, Amin BP (2025) Optimized hydrothermal alteration mapping using hybrid DWT-2D/MAD algorithm on ASTER imagery. Minerals 15(6): 626.
12. Orynbassarova E, Ahmadi H, Adebiyet B, Bekbotayeva A, Abdullayeva T, et al. (2025) Mapping alteration minerals associated with aktogay porphyry copper mineralization using landsat-8 and aster. Minerals 15(3): 277.
13. Chen Qi, Cai D, Zhao Z, Yang X, Wang Y, et al. (2025) Alteration information extraction and mineral prospectivity mapping using multisource remote sensing data. Remote Sensing 17(13): 2178.
14. Alarifi SS, Abdelkareem M, Abdalla F, Abdelsadek IS, Gahlan H, et al. (2022) Fusion of multispectral remote-sensing data through GIS-based overlay method for hydrothermal mineral resources. Minerals 12(12): 1577.
15. Malkani MS (2020) Mineral resources of Gilgit Baltistan and Azad Kashmir, Pakistan: An update. Open Journal of Geology 10: 661-702.
16. Sekandari M, Masoumi I, Pour AB, Muslim AM, Rahmani O, et al. (2020) Application of landsat-8, sentinel-2, aster and worldview-3 imagery for carbonate-hosted Pb-Zn deposits exploration. Remote Sensing 12(8): 1239.
17. Ali H, Rehman MU, Baig MA (2023) Evaluation of sentinel-2 and aster data for hydrothermal alteration mapping in Northern Pakistan. Journal of Geospatial Research 12(2): 101-118.

18. Chen Y, Wu L (2020) Comparative analysis of Landsat-8 and ASTER for iron oxide mineral mapping. Remote Sensing Applications: Society and Environment 17: 100289.

19. Zhang X, Li Y, Wang H (2022) Hydrothermal alteration mapping using fused aster and sentinel-2 imagery at the pulang porphyry copper deposit, Southwest China. International Journal of Remote Sensing 43(15): 5678-5702.

20. Aghdam MH (2022) Mapping hydrothermal alteration zones using aster imagery and advanced image processing techniques in the Takab-Baneh region, NW Iran. International Journal of Remote Sensing 43: 1-28.

21. Hassan M (2023) Integration of multispectral remote sensing and airborne geophysics for hydrothermal alteration mapping in the eastern desert of Egypt. Scientific Reports 13: 7318.

22. Silva R (2024) Comparative analysis of aster and sentinel-2 imagery for hydrothermal alteration mapping in the Uruguay mine, Brazil. Revista de Gestão Social e Ambiental 18: e6142.

23. Adetunji O (2024) Integrated aster and airborne radiometric datasets for hydrothermal alteration mapping in the igarra schist belt, Nigeria. International Journal of Engineering Sciences and Knowledge Applications 4: 1-17.

24. Elsheikh A (2025) Machine learning-assisted multisensor remote sensing for hydrothermal alteration mapping at the fatira mine, Egypt. Geological Journal.

25. El Hachimi Y (2025) Advanced aster spectral processing for hydrothermal alteration mapping and copper prospectivity in the anti- atlas, Morocco. The Egyptian Journal of Remote Sensing and Space Sciences.

26. Rojas D (2025) Integrated aster, sentinel-2, and landsat-9 remote sensing for hydrothermal alteration mapping in Northern Chile. Journal of South American Earth Sciences 142: 105214.

27. Hosseini A (2026) Deep learning-based hydrothermal alteration mapping using sentinel-2 imagery in the Zafarghand region, Iran. Scientific Reports 16: 36349.

28. Kruse FA, Anne BL, John WB, Heidebrecht KB, Shapiro AT, et al. (1993) the spectral image processing system (sips): Interactive visualization and analysis of imaging spectrometer data. Remote Sensing of Environment 44: 145-163.

29. Yoshik N (2003) A stabilized vegetation index and several mineral indices using aster data. In Proceedings of the IEEE International Geoscience and Remote Sensing Symposium (IGARSS).

30. Beiranvand PA, Hashim M (2015) Hydrothermal alteration mapping using landsat-8 and aster data. Ore Geology Reviews 65: 780-796.

31. Rowan LC, John CM (2003) Lithologic mapping in the mountain pass, California area using aster data. Remote Sensing of Environment 84 (2003): 350-366.

32. Sabins FF (1999) Remote sensing for mineral exploration. Ore Geology Reviews 14(3): 157-183.

33. Meer Freek VD, Werff HVD, Ruitenbeek FV, Hecker CA, Bakker WH, et al. (2012) Multi and hyperspectral geologic remote sensing: A review. International Journal of Applied Earth Observation and Geoinformation 14: 112-128.

34. Wei G, Cheng Q, Jing L, Li W (2022) Multisource remote sensing for hydrothermal alteration mapping: recent advances and future perspectives. Ore Geology Reviews 146: 104955.

35. Zhang X, Li Y, Wang H (2024) Multi-sensor remote sensing integration for hydrothermal alteration mapping in complex geological terrains. International Journal of Applied Earth Observation and Geoinformation 128: 103720.

36. Khan MA, Dar AR, Qureshi NA (2018) Remote sensing-based mapping of alteration zones in the Western Himalayas. Geosciences Journal 22(4): 635-649.

37. Martínez-Pérez M, Bonifazi G, Serranti S (2021) Spectral characterization of hydrothermal alteration minerals using aster data. Ore Geology Reviews 131: 104008.

38. Carvalho M, Cardoso-Fernandes J, González FJ, Teodoro AC (2025) Comparative performance of sentinel-2 and landsat-9 data for raw materials exploration. Remote Sensing 17(2): 305.

39. Jialiang T (2021) Mineral prospectivity mapping using machine learning and multi-source geo-information. Minerals 15(10): 1050.

40. Bakhberde A, Orynbassarova E, Alpysbay M, Kuznetsova I, Yerzhankyzy A, et al. (2025) Machine learning for hydrothermal alteration zoning using remote sensing data: Koldar massif case study. ISPRS Annals 48: 1-8.

41. Nguyen TT, Pham HV, Le TH (2022) Using Sentinel-2 imagery for clay mineral mapping in tropical zones. International Journal of Applied Earth Observation and Geoinformation 109: 102782.

42. Singh A, Manzoor M (2022) Multi-sensor remote sensing approach for hydrothermal alteration mapping: Ladakh region case. Journal of Remote Sensing and GIS 14(1): 45-60.

43. Zhao Y, Zhang L, Luo X (2019) Assessment of aster and landsat-8 oli data for hydrothermal alteration minerals in tibet plateau. Remote Sensing 11(12): 1472.

44. Khan AR, Mahmood ST (2025) Integration of sentinel-2 and aster data for mapping hydrothermal alteration zones in the northern himalayas. Remote Sensing Applications: Society and Environment 101950.

45. Rahman F, Iqbal MS, Ali Z (2026) Deep learning-based mineral prospectivity mapping using multispectral satellite data in arid terrains. Ore Geology Reviews 107420.

46. Mahnaz M, Katibeh H, Bahrami Y, Pour AB (2026) Metaheuristic-optimized machine learning framework for remote sensing-based alteration mapping of porphyry copper systems. Scientific Reports 16.

47. Chunya Z, Huang S, Zhang B, Shen Y, Yalikun Y, et al. (2026) Mineral prospectivity mapping based on remote sensing and machine learning in the Hatu area, China. Minerals 16(2): 144.

48. Mubashir H, Li H, Hussain M, Yuan P (2026) Emerging trends in remote sensing technologies for mineral resource mapping: An updated review. Applied Geomatics 18(3): 123.

49. Kamen B, Popov K, Velev S (2026) Integrated satellite and drone-based remote sensing for mapping porphyry and epithermal deposits in the Panagyurishte Ore District, Bulgaria. Geological Society, London, Special Publications 559(1): 2025-2036.

50. Ibrahim D, Ousaid L, Harroud A, Mihraje AI, Benamara A (2026) Ground magnetic survey and remote sensing for structural framework analysis and hydrothermal alteration of copper mineralization in the Izeroualen area, Western high atlas, Morocco. Mediterranean Geoscience Reviews pp. 1-18.

51. Hassan O, Azer MK, Zaky KS, Ali S, Farahat ES, et al. (2026) Integrating multi-source remote sensing, field work, and petrography for automatic lithological mapping and mineralization potential in the Gabal El-Faraid, Egypt. Scientific Reports 16(1): 17370.